UNIVERSITÀ DEGLI STUDI DI TORINO

Department of Molecular Biotechnology and

Health Sciences

Ph.D. program in

"Molecular Medicine"

XXXIV cycle

Phosphoinositide conversion inactivates R-RAS

and drives metastases in breast cancer

Huayi Li

Tutor: Prof. Emilio Hirsch

Coordinator: Prof. Francesco Novelli

Academic Years: 2018-2022

Table of Contents

Abstract

Breast cancer is the most prevalent cancer and a major cause of death in women worldwide. Although early diagnosis and therapeutic intervention significantly improves patient survival rate, metastasis still accounts for most deaths. Here we report that, in a cohort of more than 2000 patients with breast cancer, overexpression of PI3KC2α occurs in 52% of cases and correlates with high tumor grade as well as increased probability of distant metastatic events, irrespective of the subtype. Mechanistically, we demonstrate that PI3KC2α synthetizes a pool of PI(3,4)P2 at focal adhesions that lowers their stability and directs breast cancer cell migration, invasion, and metastasis. PI(3,4)P2 locally produced by PI3KC2α at focal adhesions recruits the Ras GTPase activating protein 3 (RASA3), which inactivates R-RAS, leading to increased focal adhesion turnover, migration and invasion both in vitro and in vivo. We eventually provide proof-of-concept that inhibiting PI3KC2α or lowering RASA3 activity at focal adhesions significantly reduces the metastatic burden in PI3KC2α-overexpressing breast cancer, thereby suggesting a novel strategy for anti-breast cancer therapy.

Keywords: breast cancer, metastases, migration, focal adhesions, PI3KC2α, R-RAS, RASA3

1. Introduction

Metastasis is a leading cause of mortality in cancer patients which results from a multistep process characterized by increased migration and invasion of cancer cells [1, 2]. Such phenotype requires the rearrangement of the cytoskeleton and abnormal cell adhesion including disassembly of focal adhesions at the rear of the cells [3, 4]. Focal adhesions are large macromolecular complexes that link actin cytoskeleton to the extracellular matrix to provide traction, thereby enabling cell migration [5, 6]. In normal and malignant cells, focal adhesion kinase (FAK), a non-receptor tyrosine kinase, is an essential regulator of focal adhesions through its kinase activity and scaffolding functions [7]. Increased FAK expression and activity are often associated with metastasis and poor clinical outcome in cancer patients, highlighting FAK as a potential determinant of cancer progression [8, 9]. However, the molecular mechanisms controlling FAK activation and focal adhesion dynamics in breast cancer metastasis remain elusive.

Phosphoinositides (PIs) are lipid signaling molecules with fundamental roles in many aspects of cell physiology [10]. PIs, together with GTPases, promote the anchoring of effectors to distinct membranes and mediate the activation of both GEFs (guanine nucleotide exchange factors) and GAPs (GTPase-activating proteins) after membrane-association through their PI-binding sites [11]. Increasing evidence suggests that PI(3,4)P2, can regulate membrane ruffle [12], podosome [13], lamellipodia and invadopodia formation and maturation [14-16] in different cellular models. For example, lack of PI(3,4)P2 alters focal adhesion dynamics in MDA-MB-231 breast cancer cells [17]. Similarly, class II PI3K α (PI3KC2α), a lipid kinase synthetizing PI(3,4)P2 mostly at the plasma membrane, is overexpressed and associated with poor prognosis in breast cancer [18]. Whether PI3KC2α overexpression and increased PI(3,4)P2 production in breast cancer increase metastatic spreading is unclear.

Here, we unveil a PI(3,4)P2-selective role in the control of focal adhesion stability in breast cancer cells. Based on our recently solved PI3KC2α crystal structure[19], we identified a helical bundle domain in the N-terminal region of PI3KC2α that is directly involved in its localization to focal adhesions. In cells overexpressing PI3KC2α, PI(3,4)P2 accumulates at focal adhesions where it recruits the Ras-GAP, RASA3 (GAP1IP4BP, R-Ras GAP). Although Ras GTPases superfamily are always considered as the notorious oncogenesis, for the controversial R-Ras, there are several studies from bench to clinics talking about R-Ras increasing anti-tumor growth and impairing cancer migration [43, 63]. Therefore, the roles of RASA3, R-Ras specific GAP are still enigmatic. Interestingly, we in this study identified that PI3KC2α derived PI(3,4)P2 pool predominantly recruited the local RASA3 by its PH domain at focal adhesion. Thus, increased localization of RASA3 at focal adhesions leads to R-RAS inactivation and reduced focal adhesion stability, promoting cell migration and invasion. Finally, our data indicates that reduction in RASA3 activity is sufficient to prevent metastasis in both cellular and animal models of breast cancer.

2.Material and Methods

Human Subjects

To assess the clinical relevance of PI3KC2α expression to breast cancer, we analyzed a series of 1779 operable breast cancer patients, available on tissue microarray (TMA), who underwent surgery at the European Institute of Oncology (IEO) in Milan from years 1997 to 2000. Details were previously shown [18]. The study was approved by the Institutional Review Board of the European Institute of Oncology (Milan, Italy) and informed consent was obtained from all subjects.

Cell lines

MCF7 was maintained in RPMI-1640 medium (Gibco) supplemented with 10% fetal bovine serum (FBS) and 1% Penicillin-Streptomycin (10,000 U/mL). SKBR3, MDA-MB468, T47D, BT474, BT549, MDA-MB-231, HEK293T, COS-7 and mice mammary tumor cell lines (67NR, 168FRAN, 4TO7, 4T1) were grown in Dulbecco's modified Eagle's medium (DMEM) with the same supplement as shown above. hTERT-HME1 were purchased from ATCC and cultured MEGMTM (Mammary Epithelial Cell Growth Medium) BulletKitTM (Cat. CC-3150) from Lonza/Clonetics Corporation. All cells were grown at 37°C in the humidified incubator (Thermo scientific) with 5% CO2. Cell lines were purchased from ATCC (without further authentication) and were routinely tested to exclude mycoplasma contamination. To establish cell lines stably overexpressing PI3KC2α, a PiggyBac transposomal system was used. Plasmids were designed and purchased from VectorBuilder Inc. Helper plasmid, carrying the expression of the transposase, and the transposable plasmid,

containing human PI3KC2α cDNA sequence, were transfected at 1:3 ratios (Ding et al., 2005; Kim and Pyykko, 2011) using X-tremeGENE™ HP DNA Transfection Reagent (Roche) followed by 7 days Blasticidine S hydrochloride (BSD) (Sigma, St. Louis, MO, USA) selection. Stable cell lines were routinely tested by Immunoblot for PI3KC2α expression and taken in cultured for no more than 20 passages.

Protein analysis

Cells and tissues were homogenized in lysis buffer (120 mM NaCl, 50 mM Tris-HCl pH=8, 1% Triton X-100) supplemented with 25x protease inhibitor cocktail (Roche), 50 mM sodium fluoride and 1 mM sodium orthovanadate. Lysates were cleared by centrifugation at 13,000 rpm for 15 min at 4°C. Protein concentration was determined by Bradford method and supernatants were analyzed for immunoblotting with the indicated antibodies. Membranes probed with the indicated antibodies were then incubated with HRP conjugated secondary antibodies (anti-mouse used 1:10000, anti-rabbit 1:5000, Sigma) and developed with enhances chemiluminescence (ECL, BD). GAPDH or α-tubulin were used for loading control as indicated above. The phosphorylation status of FAK and paxillin were normalized by their total levels. For immunoprecipitation (IP) assays, cells were lysed in 50 mM Tris-HCl (pH), 150 mM NaCl, 1% NP-40, 1 mM EDTA, 10% glycerol and protease and phosphatase inhibitors. 1 mg of pre-cleared extracts were incubated with 1 μg of the indicated antibody at 4°C on a rotating rack. After 1,5 hours, 15 μl of protein G-Sepharose (Amersham Biosciences, Buckinghamshire, UK) were added for 30 minutes. Samples were collected by centrifugation (13000 rpm 1 min) and washed six-times with lysis buffer. Bound protein complexes were then eluted by adding 30 μl Laemmli sample buffer. For pull-down experiment, HEK293T cells homogenized in lysis buffer (120 mM NaCl, 50 mM Tris-HCl pH=8, 1% Triton X-100) supplemented with 25x protease inhibitor cocktail (Roche), 50 mM sodium fluoride and 1 mM sodium orthovanadate. Lysates were cleared by centrifugation at 13,000 rpm for 15 min at 4°C. 1mg of cell lysate was incubated with 15 μl of recombinant

protein coupled with glutathione Stransferase agarose (GE, Buckinghamshire, UK) for 1 hour at 4°C. Beads were washed four times with 1 ml of reaction buffer and analyzed by Immunoblotting after the addition of 30 μl of Laemmli buffer.

Atibodies

Anti-PI3KC2α (#22028-1-AP, Proteintech), anti-GFP (gift from Emilia Turco, University of Turin, Italy), anti α-tubulin (#2125, Cell Signaling), anti GAPDH (sc-47724, Santa Cruz Biotechnology), anti Myc-tag (#2276, Cell Signaling), anti FAK (#71433, Cell Signaling), anti p-FAK(tyr397) (#8556, Cell Signaling), anti p-FAK (tyr925) (#3284, Cell Signaling), anti Paxillin (#2542, Cell Signaling), anti p-Paxillin(tyr118) (#69363, Cell Signaling), anti HA-tag (# 26183, Thermofisher) anti R-RAS (#8446, Cell Signaling), anti RASA3 (#PA5-30445,Invitrogen), anti Rap1A/Rap1B (#4938, Cell Signaling), anti RAS (#3339, Cell Signaling), anti Vinculin (#V9131, Sigma).

Gene silencing and inhibitors

Rasa3 (5'-GCGCTTTGGGATGAAGAAT-3' and 5'CCTGAAGTTTGGAGATGAA-3') siRNAs were purchased from Horizon Discovery/Dharmacon. PI3KC2α-selective PITCOIN1 inhibitor was provided by Prof. Volker Haucke and described in Wen-Ting et al.

Plasmids

PI3KC2α and PI3KC2α-GFP PiggyBac (PB) transposomal system were purchased from VectorBuilder and mutagenized to generate PB-PI3KC2α-KD and PB-PI3KC2α-KPLP by QuikChange II Site-Directed Mutagenesis Kit (Agilent) as previously described (Posor et al., 2013). myc-PI3KC2α plasmid was previously generated (Gulluni et al.). mTagRFP-Vinculin was a gift from Michael Davidson (Addgene plasmid # 58030; http://n2t.net/addgene:58030; RRID: Addgene_58030); pmCherry-C1-FAK-HA was a gift from Anna Huttenlocher (Addgene plasmid # 35039 ; http://n2t.net/addgene:35039 ; RRID:Addgene_35039), pCGN R-Ras 38V was a gift from Adrienne Cox (Addgene plasmid # 14728 ; http://n2t.net/addgene:14728 ; RRID:Addgene_14728), GST-RBD was a gift from

Martin Schwartz (Addgene plasmid # 15247 ; http://n2t.net/addgene:15247 ;

RRID:Addgene_15247), Raf-1 GST RBD 1-149 was a gift from Channing Der (Addgene

plasmid # 13338 ; http://n2t.net/addgene:13338 ; RRID:Addgene_13338), pGEXTK-Pak1 70-

117 was a gift from Jonathan Chernoff (Addgene plasmid # 12217 ;

http://n2t.net/addgene:12217 ; RRID:Addgene_12217), GFP-TAPP1-PHx3 was kindly

provided from Prof. Gerald R V Hammond (University of Pittsburgh). GFP-PI3KC2α WT,

GFP-HBD, GFP- PI3KC2α-ΔHBD were provided from Prof. Volker Hauck and described in

Wen-Ting et al. All plasmids were tested by restriction digestion and automated DNA

sequencing. Plasmids were transfected by X-tremeGENE™ HP DNA Transfection Reagent

(Roche Applied Science, Penzberg, Germany), according to the manufacturer's instructions.

Quantitative RT-PCR

Total RNA was extracted using TRIzol reagent (Invitrogen, Carlsbad, CA). cDNA was

synthesized from 1000 ng of total RNA using cDNA reverse transcription kits (Applied

Biosystems, Foster City, CA). Relative mRNA level was analyzed by real time PCR (ABI

7900HT FAST Real-Time PCR system, Applied Biosystems, Foster City, CA) with Taqman

assays, using the Universal Probe Library system (Roche Applied Science, Penzberg,

Germany). 18S gene was used as housekeeping control. The primers are listed in Table S1.

Immunofluorescence

Immunofluorescence was performed by ice cold methanol or 4% PFA fixation of the

cells followed by standard procedures (Franco et al., 2014, Gulluni et al., 2017). Next, cells

were permeabilized with 0,1% Saponin for 5 minutes and then blocked in 2% BSA for 20

minutes, followed by the incubation with indicated primary antibodies for 60 minutes. Alexa

secondary antibody (Alexa 488, Alexa 568 or Alexa633) were used 1:1000 for 45 minutes.

Cells were stained with DAPI and examined with, Leica TCS-II SP5 or Leica TSC-II SP8

confocal microscope. Raw images were digitally processed only to normalize the background

and enhance the contrast. Z-stacks were acquired and processed with the Maximum Projection tool.

Proliferation assay

Proliferation assay was performed by using CellTiter-Glo® Luminescent Cell Viability Assay (Promega, Mannheim, Germany). Cells were seeded into 96-well plates in octuplicate at 4×10^3 cells/well by. Absorbance was measured at the indicate time points.

Single cell tracking

Transfected MCF7 cells were seeded on μ-Slide 8 Well (ibidi, Germany) and cultured overnight. Cells were maintained at 37°C and 5% CO2 and cell migration was monitored by using Leica TCS-II SP5 confocal microscope (10x objective). Cells were imaged for 24 h every 10'. To assess cell migration, speed and distance, single cells were tracked by using Manual Tracking plug-in from ImageJ.

Zebrafish strains and metastasis assay

All procedures using zebrafish (Danio Rerio) were authorized by the Ethical Committee of the University of Torino and the Italian Ministry of Health. The wild-type fish strains Tuebingen was used. Adult fish were routinely maintained under a 14h light and 10h dark photoperiod at approximately 28°C, bred and genotyped according to standard procedures. Eggs were generated by natural mating, and following fertilization were collected, treated and maintained under a 12h light and 12h dark photoperiod at 28°C. Embryos were treated with 0.003% 1-phenyl-2-thiourea (PTU, #P7629, Sigma) at 24hpf to prevent formation of melanin pigment, which could interfere with the visualization of fluorescence in the metastatic assay. Embryos and adult fish were sacrificed with a tricaine overdose. For zebrafish xenotransplantation, 48hpf wild-type zebrafish embryos were anaesthetized with 0.04 mg/ml tricaine (Sigma, St. Louis, MO, USA) before cancer cell injection. Approximately 300 Vybrant™ DiI(red) or Dio (green) labeled tumor cells were injected into the yolk sac of each embryo, and zebrafish were maintained in E3 medium for 1

h at 28°C. After confirmation of a visible cell mass at the injection site, zebrafish were maintained at 30°C for 72h in standard embryo medium (Westerfield, 1994) supplemented by 0.003% PTU, 1 g/L glucose and 5 mmol/L L-glutamine. Images was acquired by Zeiss Observer-Z1 microscope (10× objective). Due to the big size of the embryos, in the representative pictures, sequential images of each embryo were acquired and composed to show the whole embryo.

Nocodazole wash out assay

Cells were grown on glass coverslips, starved overnight in medium containing 1% serum and treated with 10 µM nocodazole in serum-free medium for 4h to depolymerize microtubules, as previously described (Ezratty et al., 2005). Nocodazole was washed-out with serum-free medium and cells were incubated at 37°C for the indicated periods of time. Subsequently, cells were fixed and prepared for immunofluorescence staining with anti-Vincullin. The number of focal adhesions per cell was quantified at all time points. Images were processed after subtracting threshold levels by the Image J software.

Focal adhesion assembly and disassembly

MCF7 were transfected with FAK–mCherry and imaged by time lapse microscopy using Leica TSC-II SP8 confocal microscope for at least 1 h. Iages were acquired every 3 minutes as previously shown [20, 21]. Regions of interest (ROI) were defined by using the imageJ ROI tool to outline individual adhesions. If the FA significantly changed size and location and moved out of the ROI over time, ROIs were redrawn to include all fluorescence. Cytoplasmic background was subtracted by using duplicated ROIs adjacent to FAs. The fluorescence intensity of FA as a function of time was evaluated from the time-lapse series, by quantifying the intensity of pixels with the Image J software. As previously described [22], FA lifetime analysis was defined as the time during which the fluorescence intensity remained above the half maximum and was calculated from the assembly and disassembly curve done using the Solver function in Excel (Microsoft). The spatiotemporal correlation of focal

adhesion with GFP-TAPP1-PHx3 or PI3KC2α-GFP as a function of time was quantified based on the focal adhesion drawn regions and the intensity of GFP-TAPP1-PHx3 or PI3KC2α-GFP was measured with the ImageJ software.

Transwell assay

For cell migration assay, 3×10^4 cells suspended in serum free medium were seeded into the upper chamber of 24-well Boyden chamber (8 μm; Corning, NY, USA), and 500 μl medium with 10% FBS was added into bottom chamber. Cell invasion assay was performed using the chambers coated with Matrigel™ (Corning). After 48 h, the non-migrated/invaded cells were removed by cotton swabs and cells migrated/invaded through the membranes were fixed with 4% paraformaldehyde for 20 min and stained with 0.5% crystal violet for 30 min (Sigma, St. Louis, MO, USA). Images of five random fields for each membrane were captured by microscope. Migrated/invaded cells were counted by Image J software.

Wound healing

Cells grown 24 well plates were subjected to serum starvation for 24 h. An approximately 0.4–0.5 mm wound was scratched by using a fine end of 0.1–10μl pipette tip followed by three times washes with PBS. Cells were cultured in serum free medium throughout the experiment to avoid cell proliferation and the wounds closure were measured as the reduction area of the wound at 0 and 36 h after making the wound.

R-RAS FRET analysis at focal adhesion

COS7 cells were transfected with Vinculin-RFP and Raichu-R-RAS FRET and cultured overnight. Next, cells were fixed in 4% PFA, washed with PBS and blocked in 2% BSA solution and imaged using an 63x objective of Leica TSC-II SP8 confocal microscope. Fret analysis were described previously [23]. In brief, we obtained images for CFP and FRET. After background subtraction was carried out, the FRET/CFP ratio was depicted using ImageJ software, and the image resulting was used to represent FRET efficiency. FRET ratio at the

focal adhesion was quantified using ImageJ software. Raichu-R-RAS FRET probes were kindly provided from Prof. Michiyuki Matsuda, Kyoto University [24].

Gelatin degradation assay

Cells were seeded on the glass coverslip coated with Oregon Green™ 488-Conjugated gelatin. After 16 hours, coverslips were collected and followed by immunofluorescence staining with Rhodamine Phalloidin and ToPRO-3. Images of five random fields for each slides were captured by microscope. Gelatin degradation area were quantified by Image J software.

Mice metastatic model

Female BALB/c mice (8 to 12 weeks old) weighing between 18 and 20 g were housed at $22 \pm 5°C$ in a 12-hour light/dark cycle and fed rodent chow and water freely. Orthotopic mammary fat pad implantation was performed as follows: 10^6 4T1 cells were injected (100 μl cell suspension in PBS) in the right fourth mammary gland. Tumor growth was measured every two days after day 7, and the primary tumor was removed after 14 days when it reached the 300–400 mm3 (Jyotsana et al., 2019). Mice were monitored every two day for labored breathing and primary tumor recurrence. After two weeks, mice were sacrificed and lungs were collected for H&E staining to count lung macro-metastasis nodules. For 168-FARN, 10^6 cells were injected (100 μl cell suspension in PBS) in the right fourth mammary gland. Tumor growth was measured every week until week 6 (day42). Mice were then sacrificed and lungs were collected for H&E staining to count lung macro-metastasis nodules [25]. Protein extraction from primary tumors were used to verify PI3KC2α overexpression efficiency. All the animal use followed institutional animal welfare guidelines and legislation, as approved by the local Animal Ethics Committee (Comitato di Bioetica e Valutazione, Torino, Italy).

General Experimental Approaches

All of the statistical details of experiments can be found in the figure legends, in the Results and the Methods sections, including the statistical tests used, exact value of n, what n

represents (cells, experiments) and precision measures (mean, median, SD, SEM, confidence intervals). No statistical methods were used to predetermine sample size. No samples or data points were excluded from the reported analyses. Samples were not randomized to experimental groups. Sample size was determined on the basis of our previous studies [18, 26, 27]. The investigators were not blinded to allocation during experiments and outcome assessment.

Statistical Analysis

Prism software (GraphPad) was used for statistical analysis. Significance was calculated with Student t test and one- or two-way analysis of variance tests (ANOVA) followed by Bonferroni's post hoc analysis, or Mantel Cox log-rank test where appropriate. Values are reported as the mean ± standard error of the mean (SEM). $p<0.05$ was considered statistically significant (∗), $p<0.01$ very significant (∗∗) and extremely significant $p<0.001$ (∗∗∗).

3. Results

3.1. PI3KC2α overexpression in breast cancer leads to increased cell migration, invasion and metastasis

We previously reported that reduced expression of PI3KC2α in a cohort of more than 2000 breast cancer patients initially causes impairment of tumor growth but later leads to the convergent evolution of fast-growing clones with mitotic checkpoint defects [18]. Although we first focused on patients with low PI3KC2α expression levels, a large subset of cases from the same cohort showed increased PI3KC2α expression, correlating with enhanced probability of distant-metastatic events [18]. In particular, we extracted from our previous analysis [18] the low-grade (1-2) and high-grade tumors (grade-3) of patients expressing either low or high levels of PI3KC2α and represented these data in a pie chart in **Figure 1**a. We observed that in patients with reduced PI3KC2α expression, only 26% of the tumors were scored as grade-3 (Figure 1a, upper panel and Table 1; $p<0.00001$), in agreement with our findings showing that reduced PI3KC2α is initially protective in breast cancer [18]. In contrast, in the subset of patients expressing high levels of PI3KC2α, 49% of tumors were scored as grade 3 (Figure 1a, lower panels; Table 1; odds ratio, 3.03; 95% confidence interval (CI), 2.47-3.71; $p<0.00001$), suggesting that enhanced PI3KC2α expression was linked to increased aggressiveness and metastatic spreading [18].

We therefore analyzed PI3KC2α protein expression in different human and murine breast cancer cell lines. Increased PI3KC2α protein expression was observed in cells with higher invasive ability [28] (Figure 1b). Accordingly, analysis of PIK3C2A mRNA levels

from a Cancer Cell Line Encyclopedia (CCLE) panel [29] in luminal (low aggressiveness) or basal-like/triple negative (highly aggressive) human breast cancer cell lines showed a significant correlation between high PIK3C2A expression and basal-like/triple negative subtype (Figure S1a).

To study whether increased PI3KC2α expression was sufficient to induce tumor metastasis in vivo, we focus on two murine breast cancer cell lines, 168-FARN and 4T1, respectively with low and high metastatic ability (Figure 1b) [30]. These two cell lines were engineered with a PiggyBac (PB) transposon vector to yield stable overexpression of PI3KC2α (Figure S1b) and orthotopically injected into the mammary fat pad in mice [31]. Although increased PI3KC2α levels did not induce significant changes in tumor growth (Figure S1c-l), overexpression of PI3KC2α resulted in a significant increased number of lung metastases (Figure 1c, d). This effect was particularly evident in cells with 1ow metastatic ability such as 168-FARN, where enhanced PI3KC2α expression led to more than 5-fold increase of lung metastases (Figure 1c, d).

To better understand the molecular mechanism by which PI3KC2α overexpression promotes metastasis, human breast cancer cell lines expressing low levels of PI3KC2α, like MCF7 and MDA-MB-468, were engineered with a PiggyBac (PB) transposomal vector to produce a stable overexpression of PI3KC2α (Figure S1m). After 7 days in culture, differential gene expression, including CDH1, ZEB1, SNAI1, SNAI2, MMP3, MMP9, associated with increased cell migration and invasion was observed in MCF7 and MDA-MB-468 overexpressing PI3KC2α (PB-PI3KC2α), compared to control cells (PB empty vector) (Figure 1e and Figure S1n). Accordingly, increased extracellular matrix degradation was observed in PB-PI3KC2α compared to control PB cells in both gelatin degradation assay and transwell invasion assays (Figure 1f, g and Figure S2a, b). No significant differences in cell proliferation were observed in PB-PI3KC2α compared to PB cells (Figure S1o, p).

Enhanced cell invasion is accompanied by changes in the actin cytoskeleton towards a pro-migratory phenotype [32]. To better understand if PI3KC2α overexpression triggers rearrangements in cell shape, i.e. increased number of actin protrusions, such as filopodia and lamellipodia, PB and PB-PI3KC2α MCF7 were stained for F-actin. Breast cancer cells overexpressing PI3KC2α exhibited more stress fibers and intense ruffling at the cell edges, together with increased numbers and length of filopodia without significant alteration in the cell area (Figure 1h-j, Figure S2c,d). A stronger raised numbers and length of filopodia in PB-PI3KC2α cells was observed when cells were cultured on gelatin-coated plates (Figure S2e). In line with actin cytoskeleton remodeling and increased levels of pro-migratory genes, PI3KC2α-overexpression increased the migration velocity by 3-fold and doubled the distance traveled by breast cancer cells in a cell-tracking migration assay (Figure 1k, l). Wound healing and transwell migration assays further confirmed that PI3KC2α overexpression enhances migration in both human (MCF7 and MDA-MB-468) and murine (4T1) breast cancer cell lines (Figure 1m and Figure S2f-i). Consistent with previous report [33], PI3KC2α knockdown impairs migration/invasion ability in MDA-MB-231 (Figure S2j).

Taken together, our findings demonstrate that PI3KC2α promotes breast cancer cell migration and invasion in vitro and its increased expression correlates with breast cancer metastasis in vivo.

3.2. Increased PI3KC2α expression reduced focal adhesion number and stability.

Cell migration requires the integration and coordination of specific focal adhesion dynamics at the cell front, center and rear [3, 34]. The regulation of adhesion turnover and disassembly involves a number of tyrosine kinases and phosphatases, most of which are engaged in FAK signaling pathways [3]. To investigate the mechanisms underlying the PI3KC2α-dependent cell migration in breast cancer cells, the relationship between PI3KC2α and focal adhesion dynamics was further explored. First, we analyzed the phosphorylation status of FAK in cells

overexpressing PI3KC2α in normal or pro-migratory conditions including treatment with either TGF-β or fibronectin. We observed in PB-PI3KC2α cells that phosphorylation at Tyr397, the most important site for the regulation of FAK activity [35], was significantly increased (**Figure 2**a and Figure S3a), together with enhanced phosphorylation at Tyr925 (Figure 2a and Figure S3a), which is known to regulate cross-talk between focal adhesion turnover and cell protrusion [36]. In addition, PB-PI3KC2α cells exhibited increased phosphorylation of the focal adhesion scaffold paxillin on Tyr118 (Figure 2a and Figure S3a), a phosphorylation status commonly observed in metastatic breast cancer [37].

Phosphorylation of FAK at Tyr-397 promotes cell migration by inducing disassembly of focal adhesions at the cell tail [38]. In line with this, breast cancer cells with PI3KC2α overexpression and increased phosphorylation of Tyr-397 displayed a significantly reduced number of focal adhesions without changes in size (Figure 2b), suggesting rapid focal adhesion turnover. To test this directly, we performed a focal adhesion disassembly assay [39] and measured the focal adhesion lifetime. Nocodazole treatment was used to induce focal adhesion accumulation followed by nocodazole wash-out to measure the disassembly rate. At 30 min after release from the nocodazole block, PB-PI3KC2α MCF7 showed more than 60% of focal adhesion disassembly, compared with less than 15% in PB control cells (Figure 2c), indicating faster disassembly of focal adhesions. Similar results were observed in MDA-MB-468 overexpressing PI3KC2α (Figure S3b). Finally, time lapse analysis of living cells expressing Vinculin-RFP was performed to measure the stability of focal adhesions over time. Analysis of focal adhesion lifetime showed reduced focal adhesion stability and faster focal adhesion turnover in PB-PI3KC2α cells compared to PB controls (Figure 2d, e).

Collectively, our findings demonstrate that overexpression of PI3KC2α promotes activation of the FAK signaling pathway and shortens focal adhesion lifetime by facilitating their disassembly.

3.3. PI3KC2α is recruited to the focal adhesion by the HBD region and produces PI(3,4)P2.

To better understand how PI3KC2α overexpression affects focal adhesion dynamics, its intracellular localization was analyzed. Co-expression of GFP-PI3KC2α and FAK-mCherry in MCF7 showed that the two proteins are enriched and co-localized at plasma membrane regions corresponding to lamellipodia and filopodia (**Figure 3**a). Time-lapse imaging further revealed that GFP-PI3KC2α enrichment precedes the disassembly of the focal adhesion itself as FAK-mCherry decreased immediately following the full recruitment of GFP-PI3KC2α (Figure 3b and Figure S4a). Next, we asked how PI3KC2α is recruited to focal adhesions. We took advantage of our recently described crystal structure of PI3KC2α [19] in which we identified a sequence insertion of about 100 amino acids between the RBD and the N-C2 domain that was absent in class I and class III enzymes. This domain, named helical bundle domain (HBD), displayed structural similarity with the focal-adhesion targeting (FAT) domain of Crk-associated substrate (Cas), and the F-actin binding domains of vinculin and α-catenin (Lo et al, in revision). We posited that this protein-binding domain may be responsible for the recruitment of PI3KC2α to focal adhesions. To test this hypothesis, MCF7 cells were transfected with GFP-PI3KC2α (full length), GFP-HBD or GFP-PI3KC2αΔHBD together with HA-FAK. Co-immunoprecipitation experiments showed that full length PI3KC2α or HBD alone could both interact with HA-FAK (Figure 3c and Figure S4b). Conversely, HBD deletion from full length PI3KC2α completely abolished the binding to FAK (Figure 3c). Consistently, live cell imaging showed that GFP-HBD co-localizes with Vinculin-RFP, while deletion of the HBD region from full length PI3KC2α was sufficient to displace its localization from focal adhesions (Figure S4c). Taken together, our data demonstrate that the localization of PI3KC2α to focal adhesions is mediated by a previously unidentified association of PI3KC2α with FAK via its unique HBD domain.

Once recruited to the plasma membrane, PI3KC2α undergoes a conformational change towards an active state able to synthetize PI(3,4)P2 [40]. We hypothesized that the FAK-mediated recruitment of PI3KC2α close to the plasma membrane could be responsible for the production of a selected PI(3,4)P2 pool leading to focal adhesion reduced stability. We generated breast cancer cells that co-express a GFP-TAPP1-PHx3 binding probe able to detect PI(3,4)P2 [41] and FAK-mCherry. PI(3,4)P2 showed significant co-localization with FAK and was particularly enriched at focal adhesions where PI3KC2α was overexpressed (Figure 3d). Time-lapse analysis further showed that PI(3,4)P2 is enriched at focal adhesions immediately before focal adhesion dismantling (Figure 3e), suggesting a causal role in controlling focal adhesion lifetime. To investigate whether PI(3,4)P2 directly stimulates focal adhesion turnover, we analyzed the phosphorylation status of FAK and paxillin in cells overexpressing wild type (WT), kinase inactive (KD) and KPLP-mutant PI3KC2α. Increased phosphorylation of FAK (p-Tyr397) and paxillin (p-Tyr118) was observed in cells overexpressing wild type PI3KC2α but not in KD or KPLP mutants, demonstrating that focal adhesion turnover specifically requires PI(3,4)P2 (Figure 3f). Finally, the migratory ability of cells overexpressing wild type, KD and KPLP-mutant was assessed in a wound healing assay. In agreement with reduced FAK and paxillin activation, wound closure in KD- and KPLP-expressing cells was slower than in WT controls (Figure 3g).

These results demonstrate that recruitment of PI3KC2α by its HBD region to the focal adhesion is required for PI(3,4)P2-dependent FAK/paxillin activation and cell migration (Figure 3h).

3.4. PI3KC2α-dependent PI(3,4)P2 controls R-RAS inactivation at focal adhesion.

PI(3,4)P2 has recently emerged as a crucial regulator of cell migration in Dictyostelium, where it recruits two PH-domain containing RasGAP proteins [42], suggesting that a RAS isoform and RasGAP pair may regulate mammalian cell migration in a similar manner. In

particular, alteration in R-RAS activity leads to changes in epithelial cell motility and morphology [43-45]. Thus, we determined the intracellular localization of PI3KC2α and R-RAS in breast cancer cells. Significant co-localization between GFP-PI3KC2α and R-RAS at focal adhesion was observed (**Figure 4**a and Figure S5a), suggesting a functional relationship between the two proteins. To further probe this, the R-RAS activity was evaluated in cells overexpressing PI3KC2α using pull-down assays [24, 46]. R-RAS activity was significantly reduced in PB-PI3KC2α compared with PB controls (Figure 4b), indicating that increased PI3KC2α expression leads to R-RAS inactivation. Other RAS family members were unaffected (K-, N-, H-RAS and RAP1) (Figure S5b). To challenge our findings by an independent approach, a FRET-based sensor was used to directly visualize the activation status of R-RAS at focal adhesions [24, 47]. Raichu-R-Ras FRET probe comprised a modified YFP designated as Venus, R-Ras, the RA domain of the R-Ras effector RalGDS, a modified CFP designated as SECFP. Under R-Ras activation, the intramolecular binding of R-Ras to the RA domain brings CFP into proximity with YFP, triggering a FRET increase.We transfected cells with RFP-vinculin to visualize focal adhesions together with a FRET probe and FRET activity was measured specifically at vinculin-positive regions of the cell. In line with the data from the R-RAS pull-down assay, FRET activity was strongly reduced at focal adhesions in PB-PI3KC2α cells compared with PB controls (Figure 4c). Time-lapse imaging further revealed that focal adhesion disassembly is accompanied by inactivation of R-RAS and that in PB-PI3KC2α cells, the R-RAS inactivation is faster compared to PB controls (Figure 4d, Figure S5c). These findings demonstrate that increased PI3KC2α expression leads to selective and spatiotemporal inactivation of R-RAS at focal adhesions.

To check whether R-RAS inactivation was linked to the reduced focal adhesion lifetime and increased migration observed in cells overexpressing PI3KC2α, rescue experiments using a constitutively active form of R-RAS (R-RAS 38V) were performed. First, we analyzed the number and stability of the focal adhesions. We observed that R-RAS

38V expression in PB-PI3KC2α cells restored focal adhesions number and lifetime (Figure 4e and Figure S5d-f). Second, expression of R-RAS 38V fully prevented the accelerated wound healing and decreased filopodia observed in cells overexpressing PI3KC2α (Figure 4f and Figure S6a). Furthermore, R-RAS activity was reduced only in cells expressing wild type PI3KC2α but not cells expressing either the KD or the KPLP PI3KC2α mutant, indicating that R-RAS inactivation specifically requires a PI3KC2α-dependent production of PI(3,4)P2. (Figure 4g).

Finally, to monitor motility and tissue invasiveness of PI3KC2α-overexpressing breast cancer cells in vivo, we took advantage of zebrafish model, to trace metastasis by live imaging in embryos [48]. Hence, we injected PB (green), PB-PI3KC2α (red) in 48-hpf zebrafish (Figure S6b). As expected, we observed increased incidence of metastases and of disseminated foci in fish injected with PB-PI3KC2α breast cancer cells (Figure 4h, i and Figure S6b). Conversely, overexpression of R-RAS 38V in PB-PI3KC2α cells or treating PB-PI3KC2α cells with PI3KC2α selective inhibitor, PITCOIN [13], was sufficient to block cell spreading (Figure 4h, i).

Collectively our data point to a specific requirement of PI(3,4)P2 at focal adhesions to coordinate R-RAS activity, focal adhesion stability and cell migration (Figure 4j).

3.5. R-RAS inactivation is mediated by PI(3,4)P2-dependent RASA3 accumulation at focal adhesions.

The ability of R-RAS to switch between the active and inactive state is regulated by the balance between GEFs and GAPs activity [49]. Our observation of reduced R-RAS activity points to a selective recruitment of a RasGAP able to interact with PI(3,4)P2 at focal adhesions. A potential candidate is the RasGAP RASA3, which constitutes a component of the PI(3,4)P2 interactome [50]. Localization of RASA3 was then analyzed by immunofluorescence in breast cancer cells. Significant co-localization between RASA3 and

PI(3,4)P2 (stained with GFP-TAPP1-PHx3 probe) was observed at vinculin-positive focal adhesions (**Figure 5**a and Figure S6c). Accordingly, cells overexpressing PI3KC2α with increased PI(3,4)P2 levels showed a 2-fold increase in RASA3 enrichment at focal adhesions (Figure 5b and Figure S6d). Coherently, RASA3 knockdown in cells overexpressing PI3KC2α restored R-RAS activation, demonstrating a functional relationship (Figure 5c, d).

To link the recruitment of RASA3 at focal adhesions with its GAP activity towards R-RAS, we performed a FRET analysis to measure R-RAS activation. While in PB-PI3KC2α cells, R-RAS activity was significantly reduced at focal adhesions, knock-down of RASA3 was sufficient to restore R-RAS activity to levels comparable to control PB cells (Figure 5e). Therefore, RASA3 controls R-RAS activation at focal adhesion in a PI(3,4)P2-dependent manner. Then we checked whether RASA3-mediated inactivation of R-RAS directly affects cell migration in wound healing assays. While PB-PI3KC2α cells showed a fast closure of the wound, concomitant down-modulation of RASA3 was sufficient to slow the wound closure similar to the rate observed in control cells (Figure 5f).

Finally, to challenge our findings in an in vivo model, we used an in vivo zebrafish model [48]. To this aim, we injected PB, PB-PI3KC2α and PB-PI3KC2α together with siRNA targeting RASA3 in 48-hpf zebrafish. As expected, we observed an increased number of metastases and disseminated foci in fish injected with PB-PI3KC2α breast cancer cells. Conversely, knocking-down of RASA3 in PB-PI3KC2α cells was sufficient to block the migratory process (Figure 5g-i).

Collectively, our findings demonstrate that PI(3,4)P2-RASA3 mediated inactivation of R-RAS allows PI3KC2α-overexpressing breast cancer cells to acquire a pro-migratory and pro-invasive phenotype, leading to increased metastatic potential (Figure 5j). Moreover, we provide a proof of concept that inhibiting PI3KC2α or targeting RASA3 activity can block the metastatic spreading of breast cancer cells overexpressing PI3KC2α in vivo.

4. Discussion

By producing PI(3)P and PI(3,4)P2, PI3KC2α plays an essential role during development and its loss or inactivation leads to multiple pathological processes [26, 27, 51-53]. Besides its enzymatic activity, we recently described a scaffold function of PI3KC2α that is necessary for keeping genome integrity by preventing mitotic defects in breast cancer cells [18]. Accordingly, loss of PI3KC2α in breast cancer initially delays tumor growth but finally leads to the selection of more aggressive clones. Here we describe that, unlike patients with PI3KC2α loss, high levels of PI3KC2α correlate with tumor grade and probability of distant metastatic events in breast cancer patients. In agreement with this phenotype, we found that a PI(3,4)P2 pool synthetized by PI3KC2α at focal adhesions disturbs their stability, leading to enhanced breast cancer cell migration and invasion. Moreover, differential expression of genes involved in migration and invasion can be likely explained as a consequence of increased focal adhesion dynamics and cytoskeletal remodeling [54-56], induced by PI3KC2α overexpression. This is particularly evident in light of the fact that Class-II PI3K have never been shown to function in gene transcriptional regulation [51].

Although our model of increased tumor cell migration and invasion relies on the PI3KC2α catalytic activity, the recently described PI3KC2α HBD domain emerged as a critical region for protein-protein interaction [19]. In particular, this domain appears pivotal to the localization of PI3KC2α to cytoskeletal structures, as initially we found it to localize this kinase to the mitotic spindle by binding with TACC3 [18] and now to target PI3KC2α to focal adhesions, by promoting its association with FAK. In line with these findings, the HBD shares structural similarities with the focal-adhesion targeting (FAT) domain of Crk-associated substrate (Cas), and the F-actin binding domains of vinculin and α-catenin, both necessary and sufficient for protein localization to the focal adhesions [13]. Altogether these findings suggest that the HBD domain of PI3KC2α has a structural role as a protein-

25

interacting domain in driving fundamental association with different proteins, critically required to localize PI3KC2α activity in specific subcellular compartments.

While PI(3,4)P2 has been previously associated with increased cell migration [14, 17, 57, 58] and an inhibitory RAS-PI(3,4)P2 feedback loop was recently proposed [42], its relevance for tumor metastases in vivo remained largely elusive. Our findings point to a direct role for PI(3,4)P2 in controlling focal adhesion stability, and identified the R-Ras-GAP RASA3 as the main player in driving R-RAS inactivation during migration and invasion, both in vitro and in vivo. Based on our findings, PI(3,4)P2 produced by PI3KC2α recruits RASA3 at focal adhesions, leading to R-RAS inactivation and focal adhesion dismantling. The localization of endogenous RASA3 at focal adhesion complexes is required for cytoskeleton rearrangement and cell migration, and loss of RASA3 impairs focal adhesion turnover [20]. Importantly, our data shows that increased PI3KC2α-mediated PI(3,4)P2 production significantly reinforces the localization of RASA3 at focal adhesions.

RASA3 is known to function as a dual GAP for R-RAS and RAP1 small GTPases [59, 60]. Here we found that, at least in breast cancer epithelial cells, overexpression of PI3KC2α leads to increased PI(3,4)P2 enrichment at focal adhesion accompanied by an increased activity of RASA3 towards R-RAS. Considering that the switch of RASA3 from RAS-GAP to RAP-GAP involves its PH domain [61], we hypothesize that PI(3,4)P2 might affect this conformational change by promoting RASA3 activity in an R-RAS selective manner. Further studies are needed to better elucidate this mechanism of action.

Previous works showed that the C-terminal region of R-RAS contains a focal adhesion targeting signal and that targeting and activation of R-RAS are linked processes in the formation of focal adhesion in epithelial cells [43, 44]. Interestingly, only R-RAS-GTP is recruited to focal adhesions, enhancing both cell adhesion and cell spreading [43, 62]. Conversely, deactivation of R-RAS leads to its exclusion from focal adhesions and reduced focal adhesion stability [43]. In line with this, expression of dominant negative R-RAS (41A)

enhances migration persistence and membrane protrusion [63]. Our data further expanded these findings, showing that in breast cancer cells, the R-RAS inactivation and the consequent reduction in focal adhesion number and stability rely on PI(3,4)P2-mediated recruitment of the Ras-GAP, RASA3 to focal adhesions. We speculate that the RASA3-driven inactivation of R-RAS can be responsible for R-RAS release from the focal adhesions and their consequent destabilization and enhanced turnover, leading to increased cell migration. Additionally, the zebrafish xenograft model conclusively demonstrated that the PI3KC2α/RASA3/R-RAS axis controls breast cancer distant metastasis in vivo; nonetheless, future study in mouse models will better elucidate the importance of targeting PI3KC2α and RASA3 in metastatic breast cancer therapy.

Despite recent advances in anticancer therapies targeting the primary mammary gland tumor, treating metastatic breast cancer has remained challenging. Therefore, identification of new druggable pathways promoting metastasis remains an unmet medical need. The finding of the crosstalk between PI3KC2α and RASA3 identifies two potential therapeutic targets. On the one hand, development of more potent and selective PI3KC2α inhibitors might open new therapeutic strategies for metastatic breast cancer. On the other, GAPs like RASA3 are potentially druggable and our proof-of-concept study provides evidence that inhibition of RASA3 GAP activity can significantly reduce metastasis of breast cancer irrespective of the subtype and likely even in other cancer types.

5. Figures and tables

Figure 1
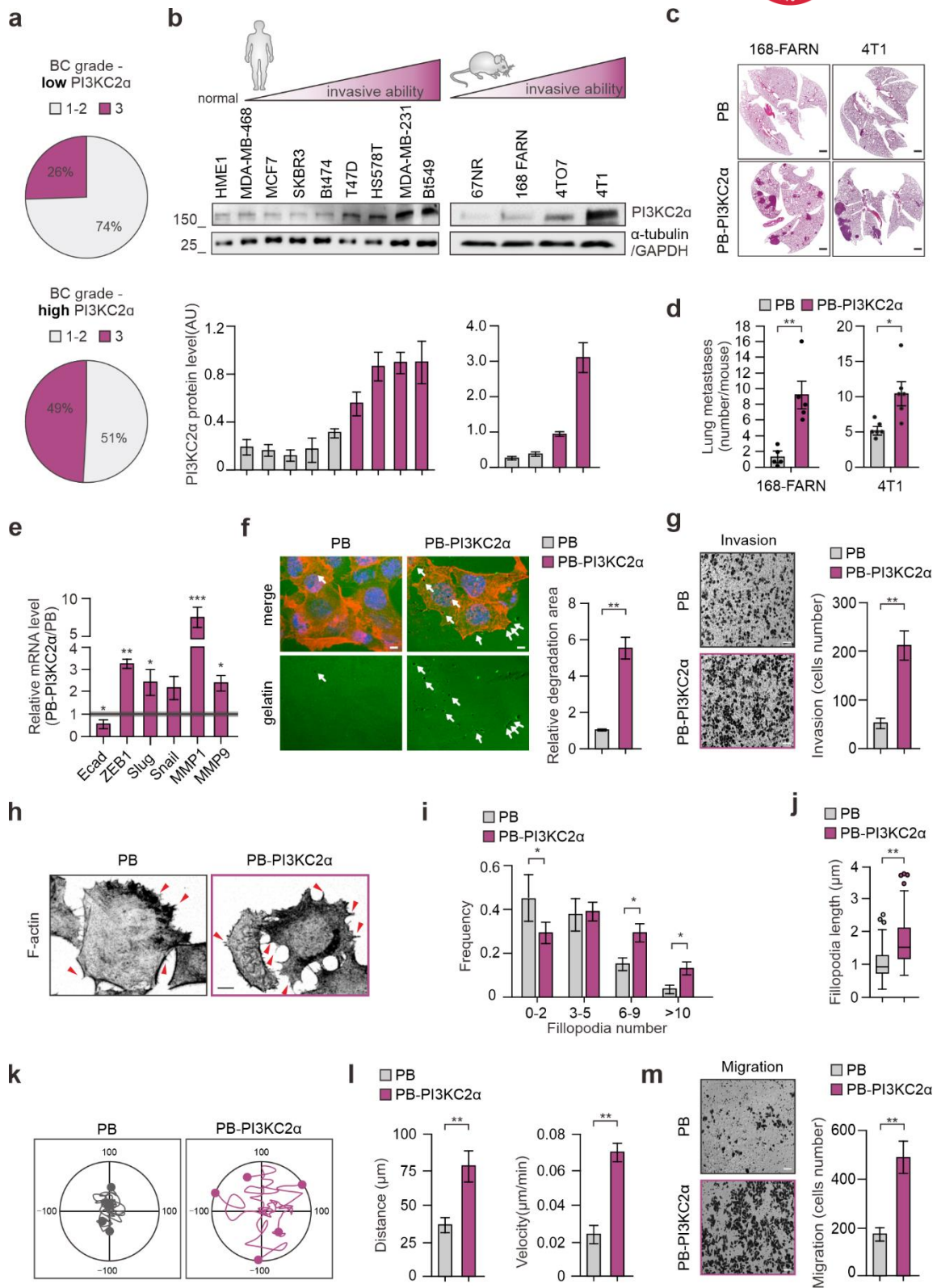
Figure 1. Overexpression of PI3KC2α in breast cancer leads to increased metastatic burden and cell migration. a) Pie chart showing breast cancer grade in either low or high PI3KC2α patients extracted from Gulluni et al Table 1[18]. b) Quantification and representative blots showing PI3KC2α protein expression normalized over α-tubulin in human BC cell lines and

normal mammary cell line HME1 (left panels). Quantification and representative blots showing PI3KC2α protein expression normalized over GAPDH in four isogenic murine BC cell lines (right panels). c, d) Lung metastasis analyzed in BALB/c mice orthotopically injected with PB or PB-PI3KC2α 168-FARN (left panels). Lung metastasis analyzed in BALB/c mice orthotopically injected with PB or PB-PI3KC2α 4T1 (right panels). Representative H&E staining are shown (c) (scale bar = 2 mm). Each dot in the graphs (d) is representative of an injected mouse (n ≥ 5). e) Real-time analysis performed on PB or PB-PI3KC2α MCF7. mRNA levels of indicated genes are reported as ratio over control. f) PB or PB-PI3KC2α MCF7 were prepared and cultured on glass coverslips covered with cross-linked gelatin overlaid with Oregon GreenTM 488. Cells were stained with phalloidin to identify actin filaments (F-actin; red) and ToPRO3 (nuclei, blue). Degraded gelatin is identified as a dark area (white arrows) on the Oregon GreenTM 488 (green) background. g) Representative pictures and quantification of Transwell invasion assay in PB and PB-PI3KC2α MCF-7; scale bar = 100 μm. h) Immunofluorescence staining using Phalloidin to detect F-actin in PB or PB-PI3KC2α MCF-7. Extensive filopodia formation can be observed in PB-PI3KC2α group as indicated by red arrow. i) Frequency distribution showing filopodia number in PB or PB-PI3KC2α MCF7. n = 162 and n = 168 cells were imaged for PB and PB-PI3KC2α MCF7, respectively, in three independent experiments. j) Filopodia length measured in PB or PB-PI3KC2α MCF7 cells. n = 46 and n = 51 cells were imaged for PB and PB-PI3KC2α MCF7, respectively, in three independent experiments. k, l) Representative cell tracks over 10 h (k) and quantification of the migration distance and speed (l) are shown. Data were analyzed using Manual Tracking plugin (ImageJ). n = 34 and n = 35 cells for PB and PB-PI3KC2α respectively. m) Representative pictures and quantification of Transwell migration assay in PB and PB-PI3KC2α MCF-7; scale bar = 100 μm. All results are shown as mean of at least three independent experiments ± SEM (n.s., no significance, *P<0.05; **P<0.01; ***P<0.001).

31
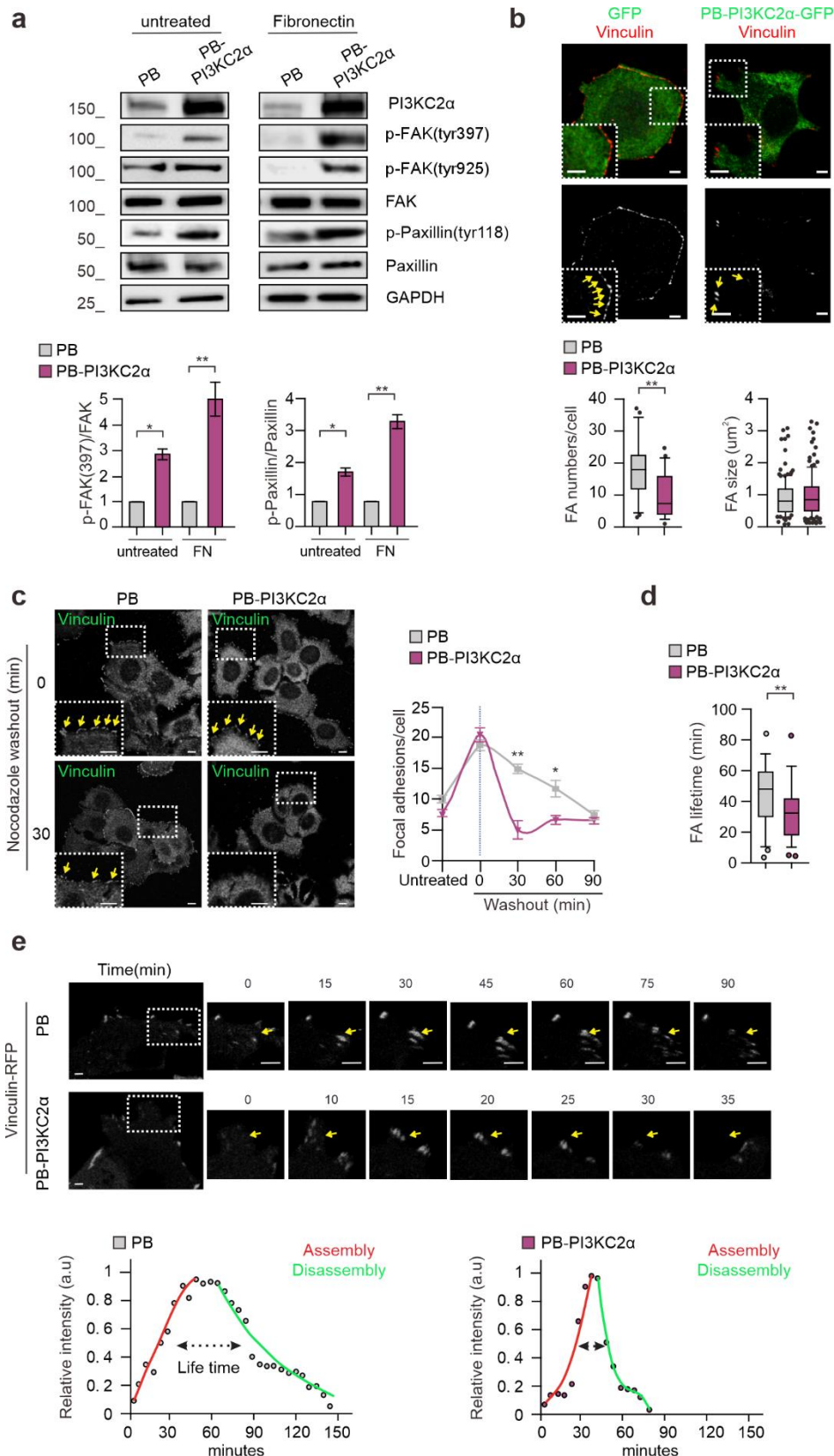
Figure 2

Figure 2. Increased PI3KC2α expression enhanced focal adhesion disassembly rate. a)

Immunoblot analysis (upper panel) and p-FAK(tyr397) and p-Paxillin(tyr118) protein

quantification (lower panels) performed on untreated, TGF-β or Fibronectin treated PB or PB-

PI3KC2α MCF7. b) Immunofluorescence performed on PB-GFP and PB-PI3KC2α-GFP MCF7 showing Vinculin (red) and GFP (green). Quantification of focal adhesions number and size is shown in the Tukey box plots below. n = 12 cells and n = 21 for PB-GFP or PB-PI3KC2α-GFP respectively from three independent experiments. c) Nocodazole washout assay was used to assess focal adhesion disassembly time (see Experimental Section). PB and PB-PI3KC2α MCF7 were fixed at indicated time points and immunostained for Vinculin. Representative pictures (left) and quantification of focal adhesions number per cell are shown (right). At least 6 images per time point were analyzed (5–10 cells per picture). Scale bar, 10 µm. d, e) Quantification (d) of focal adhesion lifetime from time lapse performed on living cells expressing Vinculin-RFP (e) PB or PB-PI3KC2α MCF7. n ≥ 23 focal adhesions from three independent experiments. The red and green lines are respectively a logistic fit of the assembly and an exponential fit of the disassembly phase. Adhesions lifetimes are indicated by dashed arrows as defined by fluorescence intensity above the half maxim of the fit. All results are shown as mean of at least three independent experiments ± SEM (n.s., no significance, *P<0.05; **P<0.01).
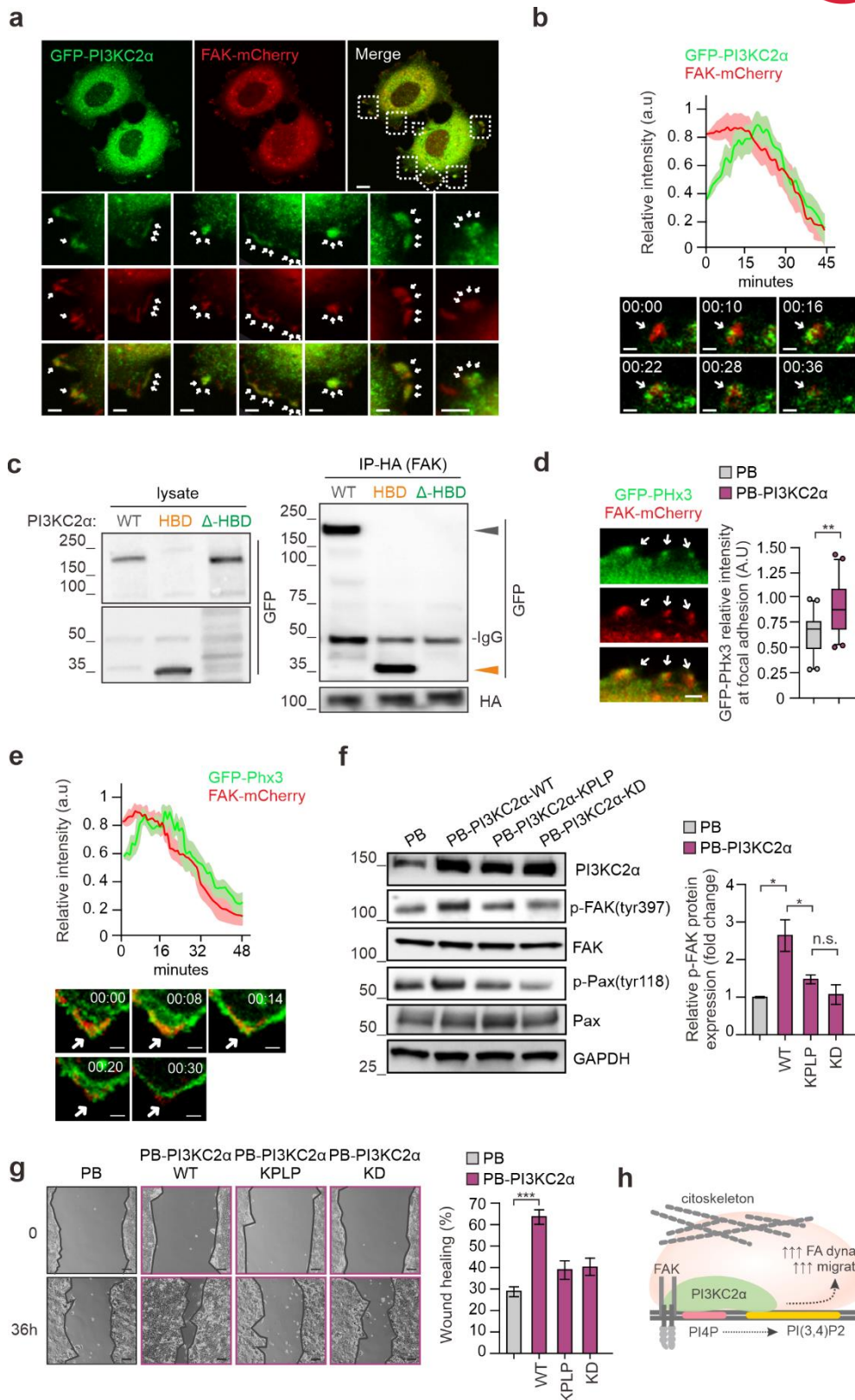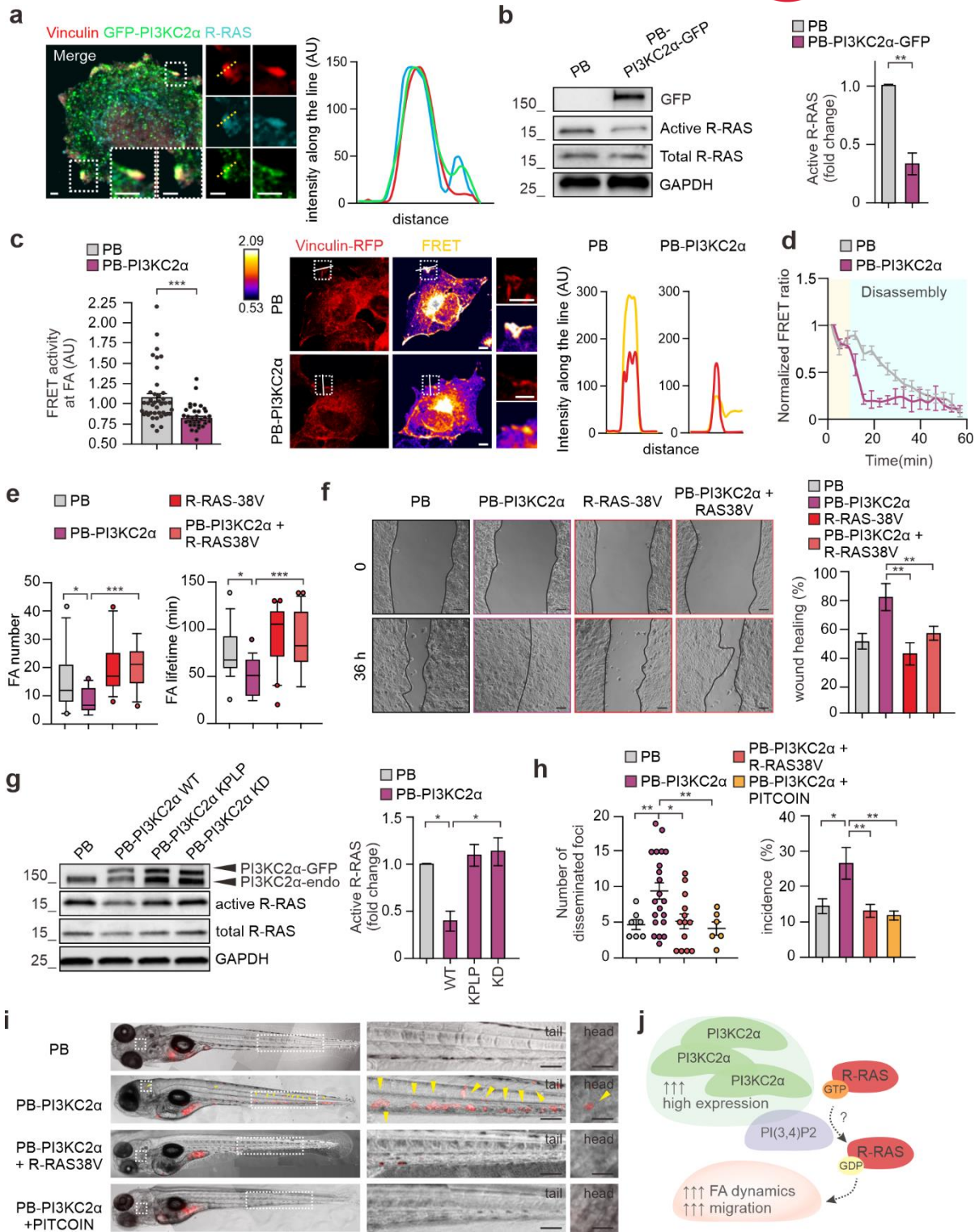
Figure 3

Figure 3. Increased PI3KC2α expression enhanced focal adhesion disassembly rate. a) Live

cell imaging performed in MCF7 expressing FAK-mCherry (red) and GFP-PI3KC2α (green).

Enlarged sections show co-localization between PI3KC2α and FAK. b) Turnover dynamics of

FAK-mCherry labeled focal adhesions (red) and GFP-PI3KC2α (green). Fluorescence intensity profiles measured as a function of time were normalized to the maximum FAK-mCherry fluorescence intensity for each focal adhesion and aligned relative to one another (n = 13 focal adhesions). c) HEK293T cells were transfected with HA-FAK and GFP-PI3KC2a (WT, HBD or HBD deleted mutants). HA-FAK was immunoprecipitated with anti-HA antibody (IP). Bound proteins were blotted with anti-GFP or anti-HA. d) Representative picture (left) and PI(3,4)P2 quantification at focal adhesion (right) in live cell imaging performed on MCF7 expressing GFP-TAPP1-PHx3 (green) and FAK-mCherry (red). n = 44 and n = 63 FAs for PB or PB-PI3KC2α respectively. Scale bar, 1 μm. e) Turnover dynamics of FAK-mCherry labeled focal adhesions (red) and GFP-TAPP1-PHx3 (green). Fluorescence intensity profiles measured as a function of time were normalized to the maximum FAK-mCherry fluorescence intensity for each focal adhesion and aligned relative to one another (n = 10 focal adhesions). f) Immunoblot analysis (left panel) and p-FAK(tyr397) and p-Paxillin(tyr118) protein quantification (right panel) performed on untreated PB or PB-PI3KC2α-WT, PB-PI3KC2α-KPLP (PI3P-producing only) or PB-PI3KC2α-KD (kinase inactive) MCF7. g) Wound healing assay performed on PB, PB-PI3KC2α-WT, PB-PI3KC2α-KPLP or PB-PI3KC2α-KD MCF7. Representative pictures are shown on left panel and quantification of the wound area closure on right panel. Scale bar, 100 μm. h) Schematic representation showing that PI3KC2α is recruited to focal adhesion trough association with FAK by its HBD region during focal adhesion turnover. Here PI3KC2α synthetizes PI(3,4)P2 required for FAK/paxillin activation and cell migration. All results are shown as mean of at least three independent experiments ± SEM (n.s., no significance, *P<0.05; **P<0.01).

Figure 4

Figure 4. PI3KC2α-dependent PI(3,4)P2 controls R-RAS inactivation at focal adhesion. a) Immunofluorescence staining performed on MCF7 showing colocalization of GFP-PI3KC2α (green) with endogenous R-RAS (cyan) and Vinculin (red). Fluorescence intensity along the dashed line is quantified on right panel. b) Pull-down assay (left) and quantification (right) showing active R-RAS in PB or PB-PI3KC2α MCF7. c) PB and PB-PI3KC2α COS7 cells transiently expressing Raichu-R-RAS FRET probe showing R-RAS activity (higher FRET ratio) at the focal adhesion stained by Vinculin-RFP. FRET ratio at focal adhesion is quantified by using ImageJ software (left panel). Representative FRET ratio images are shown together with intensity along the line (right panels). n=40 and n=32 focal adhesions for PB or PB-PI3KC2α respectively. Scale bar = 10 μm. d) Timelapse analysis of normalized R-RAS FRET ratio at focal adhesions during their disassembly performed in PB or PB-PI3KC2α MCF7 expressing Vinculin-RFP and Raichu-R-RAS FRET probe. The resulting time course was normalized by dividing the ratio at each time point by the basal value at time zero, n ≥ 10 focal adhesions. e) Quantification of focal adhesion numbers and lifetime from time lapse performed on living MCF7 cells expressing Vinculin-RFP and PB, PB-PI3KC2α, R-RAS 38V or PB-PI3KC2α + R-RAS 38V respectively. n ≥ 10 focal adhesions from three independent experiments. f) Wound healing assay performed on PB, PB-PI3KC2α, R-RAS 38V or PB-PI3KC2α + R-RAS 38V MCF7. Representative pictures are shown on left panels and quantification of the wound area closure on right panel. Scale bar, 100 μm. g) Pull-down assay (left) and quantification (right) showing active R-RAS in PB, PB-PI3KC2α-WT, PB-PI3KC2α-KPLP or PB-PI3KC2α-KD MCF7. h, i) Quantification (h) and representative pictures (i) showing number of disseminated foci and incidence of metastases in 48 hpf zebrafish injected with PB, PB-PI3KC2α, PB-PI3KC2α + R-RAS 38V or PB-PI3KC2α + PITCOIN MCF7. Arrows indicate metastatic foci in zebrafish tail and head. n = 27 (PB), n = 77 (PB-PI3KC2α), n = 94 (PB-PI3KC2α + R-RAS 38V) and n = 42 (PB-PI3KC2α + PITCOIN) zebrafish. Scale bar = 200 μm or 25 μm in enlarged sections. j) Schematic

representation showing that PI3KC2α overexpression reduces R-RAS activation due to PI(3,4)P2 production at focal adhesion. This results in increased focal adhesion disassembly rate and enhanced cell migration both in vitro and in vivo. All results are shown as mean of at least three independent experiments ± SEM (n.s., no significance, *P<0.05; **P<0.01; ***P<0.001).
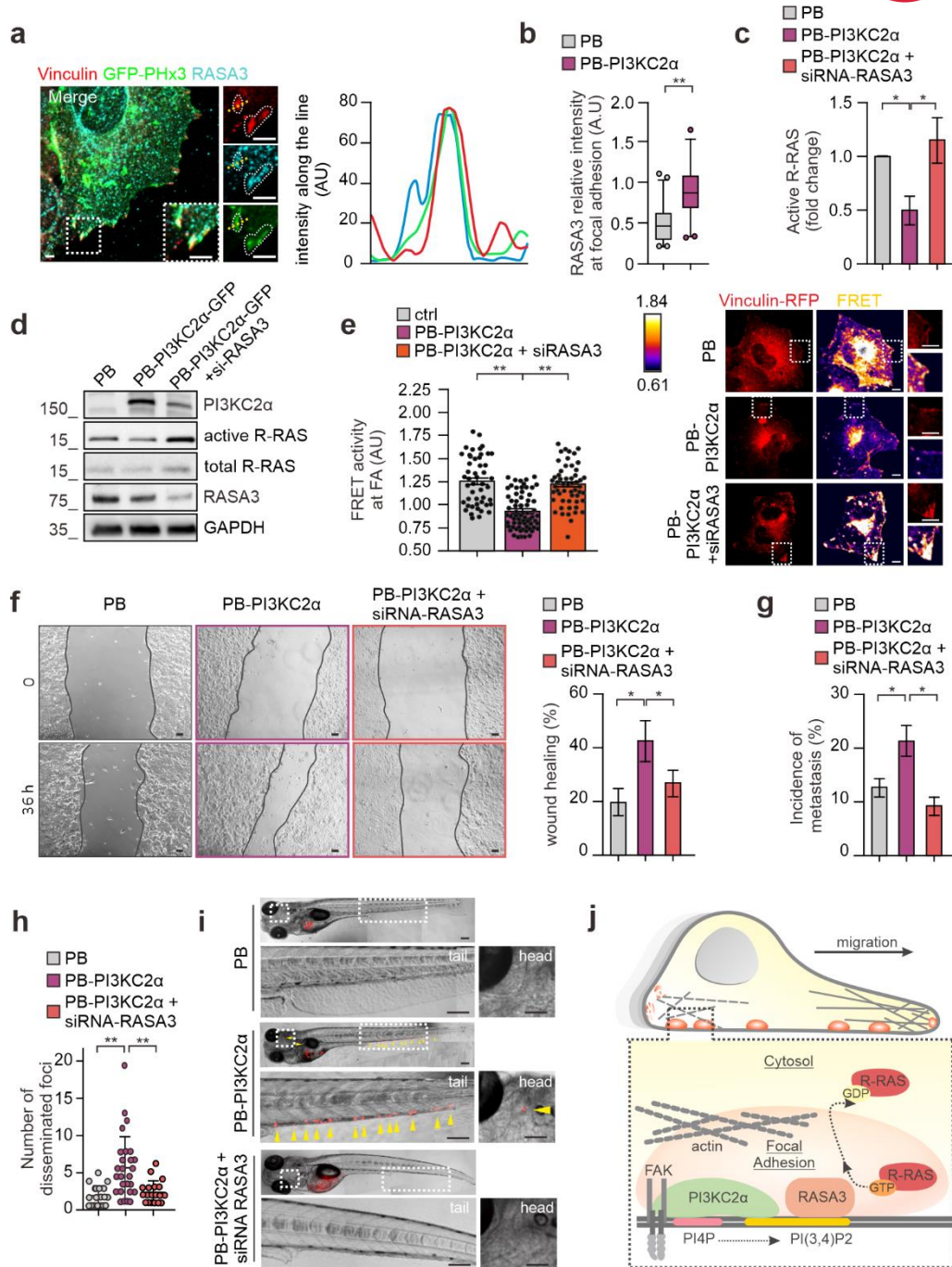
Figure 5

Figure 5. R-RAS inactivation is mediated by PI(3,4)P2-dependent RASA3 accumulation at

FAs. a) Immunofluorescence staining performed on MCF7 showing colocalization of GFP-

TAPP1-PHx3 (green) with endogenous RASA3 (cyan) and Vinculin (red). Fluorescence intensity along the dashed line is quantified on right panel. b) Immunofluorescence quantification of RASA3 intensity at focal adhesion in PB or PB-PI3KC2α MCF7 (n=44 and n = 63 focal adhesions for PB or PB- PI3KC2α respectively). c, d) Quantification (c) of pull-down assay (d) showing active R-RAS in PB, PB-PI3KC2α and PB-PI3KC2α + siRNA-RASA3 MCF7. e) PB, PB-PI3KC2α and PB-PI3KC2α + siRNA RASA3 COS7 cells transiently expressing Raichu-R-RAS FRET probe showing R-RAS activity (higher FRET ratio) at the focal adhesion stained by Vinculin-RFP. FRET ratio at focal adhesion is quantified by using ImageJ software (left panel). Representative FRET ratio images are shown (right panels). n=59 (PB), n=82 (PB-PI3KC2α) and n = 60 (PB-PI3KC2α + siRNA-RASA3) focal adhesions. Scale bar = 10 μm. f) Wound healing assay performed on PB, PB-PI3KC2α or PB-PI3KC2α + siRNA-RASA3 MCF7. Representative pictures are shown on the left panels and quantification of the wound area closure on right panel. Scale bar, 100 μm. g, h, i) Quantification (g, h) and representative pictures (i) showing incidence of metastases (g) and number of disseminated foci (h) in 48 hpf zebrafish injected with PB, PB-PI3KC2α, PB-PI3KC2α + siRNA-RASA3 MCF7. Arrows indicate metastatic foci in zebrafish tail and head (i). n = 81 (PB), n= 87 (PB-PI3KC2α) and 94 (PB-PI3KC2α + siRNA-RASA3) zebrafish. Scale bar = 200 μm or 25 μm in enlarged sections. j) Schematic representation showing that PI3KC2α produces PI(3,4)P2 at focal adhesion which recruits RASA3 that in turns inactivates R-RAS. This results in increased focal adhesion disassembly rate and enhanced cell migration both in vitro and in vivo. All results are shown as mean of at least three independent experiments ± SEM (n.s., no significance, *P<0.05; **P<0.01;).

Table 1. Association between PI3KC2α status and tumor grade.

	Grade 1-2	Grade 3	Column Totals	Odds Ratio	95 % CI	Head 5 [units]
PI3KC2α low n (% row)	627 (74%)	216 (26%)	843			
PI3KC2α high n (% row)	442 (51%)	462 (49%)	904	3.03	2.47 to 3.71	P < 0.00001
Row Totals	1069	678	1747			

Supporting Information
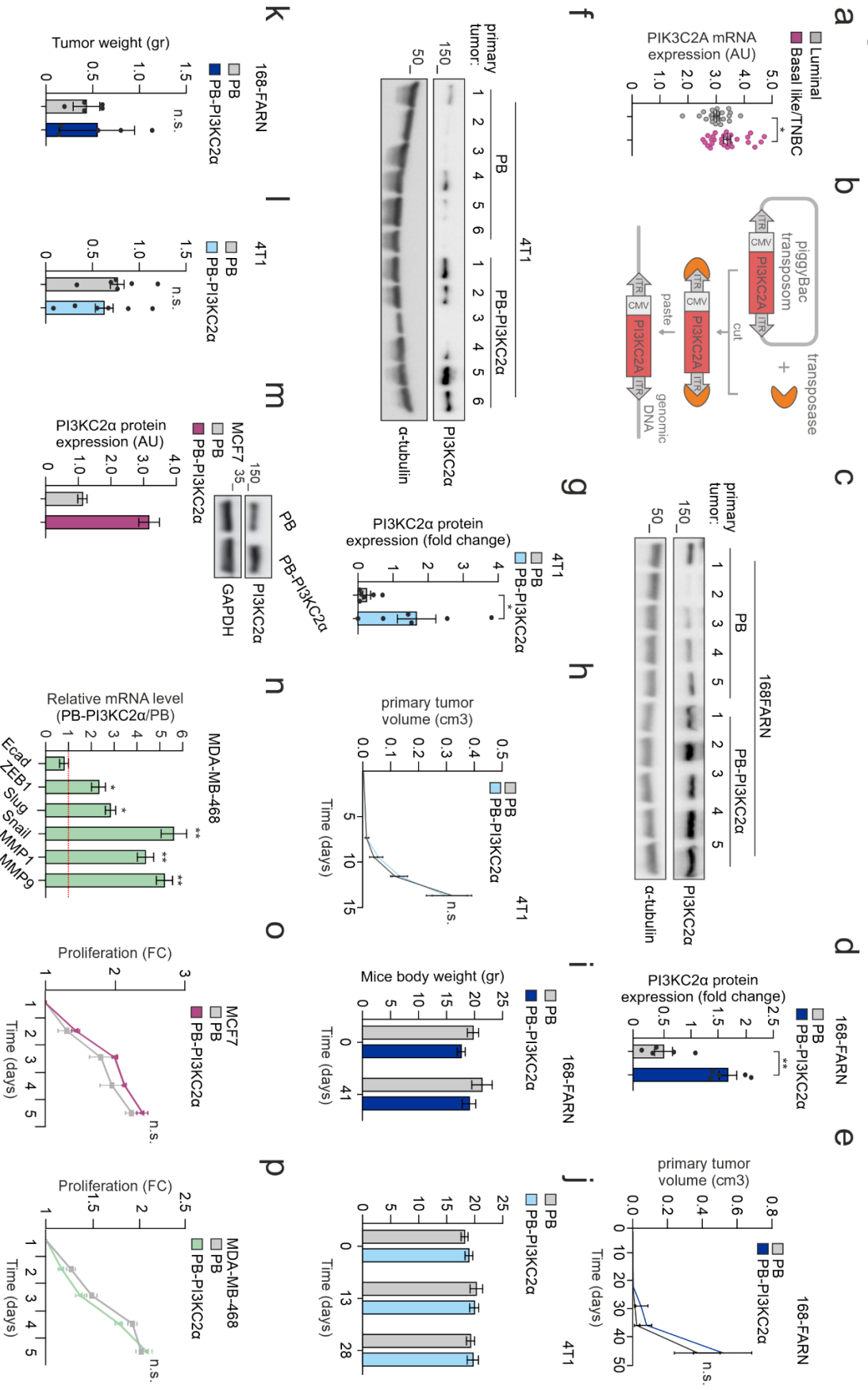
Figure S1

Figure S1. a) Analysis of PI3KC2α mRNA level in luminal (n = 22) and basal/triple-negative (n = 27) breast cancer cell lines available in CCLE. b) Schematic representation depicting the PiggyBac (PB) transposomal system used to produce stable overexpression of PI3KC2α. ITR: inverted terminal repeats; CMV: cytomegalovirus (CMV) immediate early enhancer and promoter. c, d) Representative immunoblots (c) and quantifications (d) showing PI3KC2α protein expression in 168-FARN derived primary tumors. Each dot in graphs (d) is representative of an injected mouse (n =5). e) Analysis of 168-FARN derived primary tumor volume (n = 5). f, g) Representative immunoblots (f) and quantifications (g) showing PI3KC2α protein expression in 4T1 derived primary tumors. Each dot in graphs (g) is representative of an injected mouse (n = 6). h) Analysis of 4T1 derived primary tumor volume (n = 6). i, j) Analysis of mice body weight in 168-FARN group (i, n = 5) and 4T1 group (f, n = 6). k, l) Analysis of primary tumor weight in 168-FARN group (i, n = 5) and 4T1 group (f, n = 6). m) Representative blots and quantification of PI3KC2α protein level in PB and PB-PI3KC2α MCF7. n) Real-time analysis performed on PB or PB-PI3KC2α MDA-MB-468. mRNA levels of indicated genes are reported as ratio over control. o, p) Proliferation analysis performed in PB or PB-PI3KC2α MCF7 (o) and PB or PB-PI3KC2α MDA-MB-468 (p). All results are shown as mean of at least three independent experiments ± SEM (n.s., no significance, *P<0.05; **P<0.01).

Figure S2
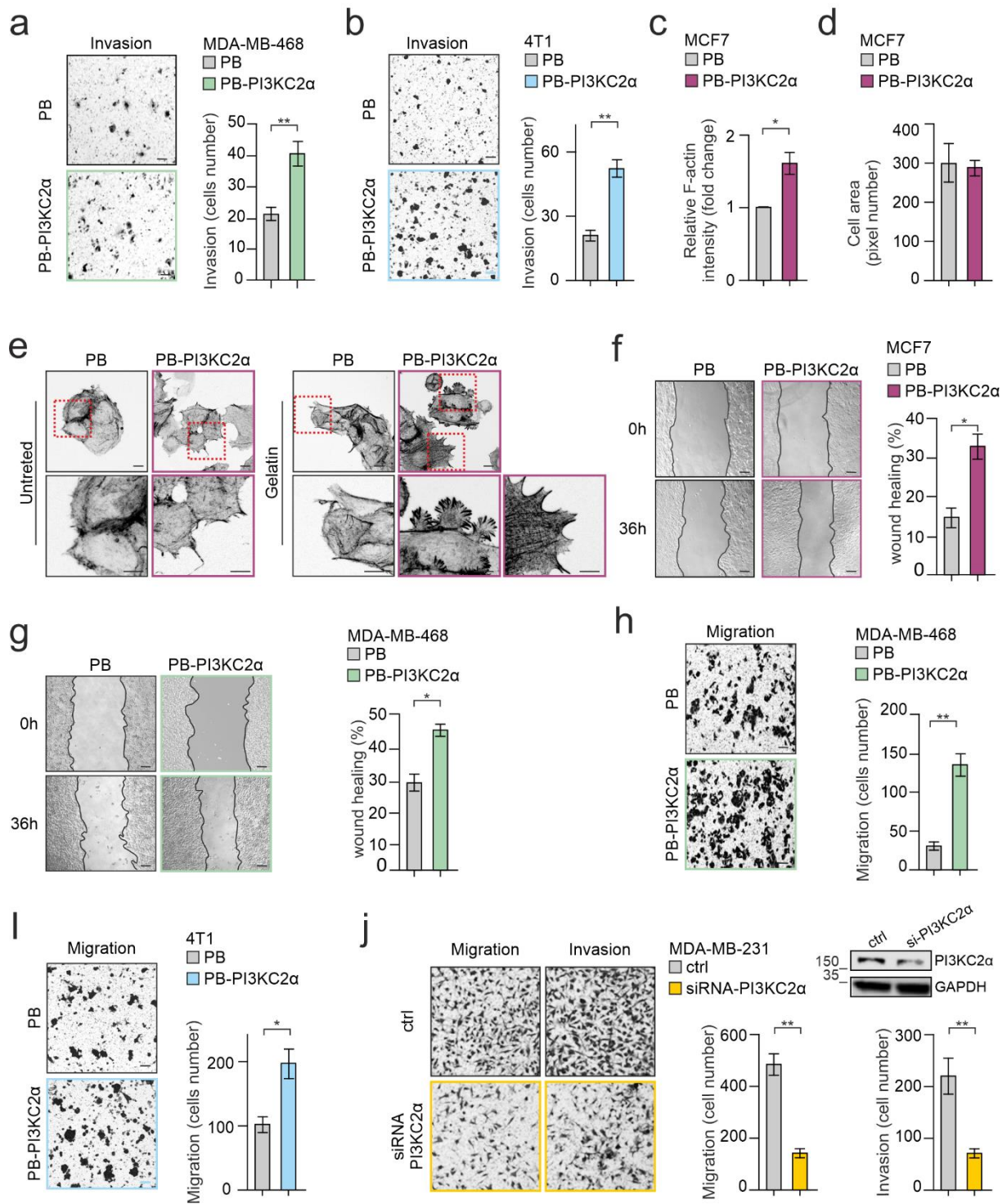
**Figure S2.** a, b) Transwell invasion assays performed in PB or PB-PI3KC2α MDA-MB-468(a) and PB or PB-PI3KC2α 4T1(b). Scale bar = 100 μm. c) F-actin intensity measured in PB or PB-PI3KC2α MCF7 cells. n = 46 and n = 51 cells were imaged for PB and PB-

44

PI3KC2α MCF7, respectively, in three independent experiments. d) Cell area measured in PB or PB-PI3KC2α MCF7 cells stained for Phalloidin. n = 46 and n = 51 cells were imaged for PB and PB-PI3KC2α MCF7, respectively, in three independent experiments. e) Immunofluorescence staining using Phalloidin to detect F-actin in PB or PB-PI3KC2α MCF-7 with or without gelatin coating. Filopodia formation can be observed in the enlarged sections. f, g) Wound healing assay performed in PB or PB-PI3KC2α MCF-7 (f) and PB or PB-PI3KC2α MDA-MB-468(g). Representative pictures (left panel) and relative quantification (right panel) are shown. Scale bar = 100 μm. h, i) Transwell migration assays performed in PB or PB-PI3KC2α MDA-MB-468(h) and PB or PB-PI3KC2α 4T1(i). Scale bar = 100 μm. j) Transwell migration and invasion assay performed in MDA-MB-231 treated with control siRNA or siRNA targeting PI3KC2α. Scale bar = 100 μm. All results are shown as mean of at least three independent experiments ± SEM (n.s., no significance, *P<0.05; **P<0.01).

Figure S3
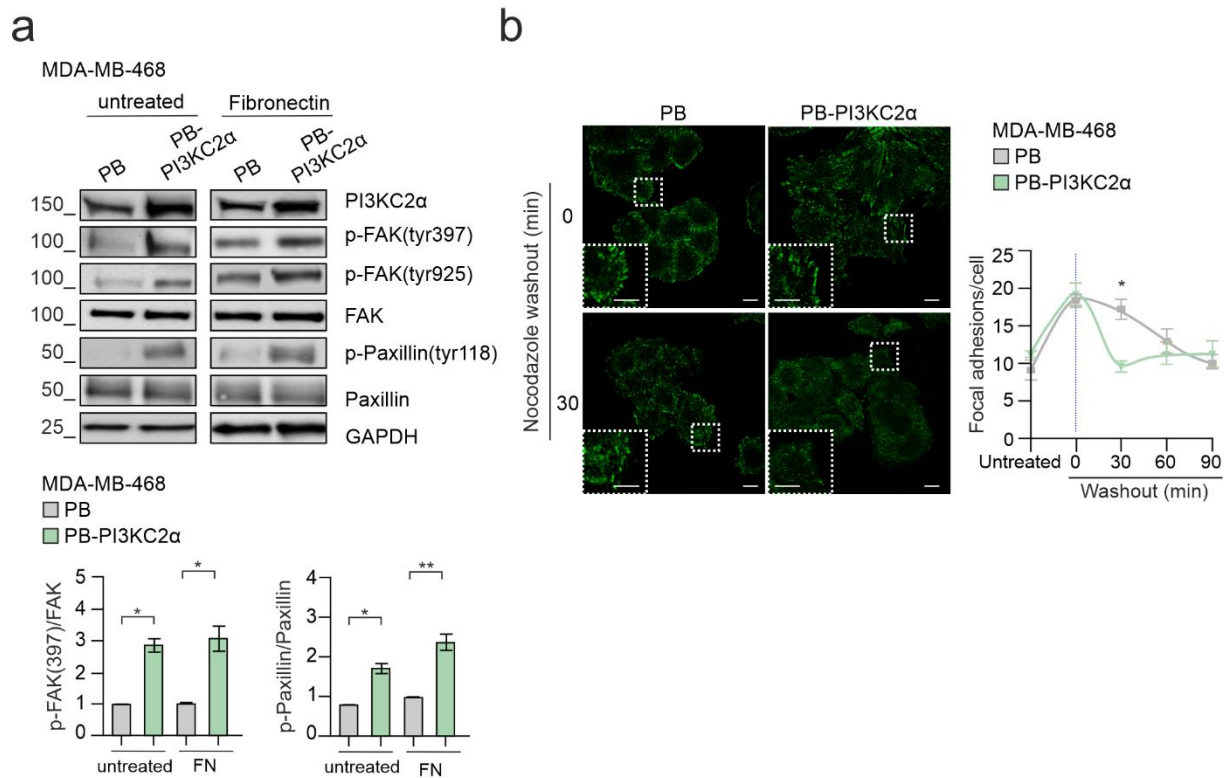
Figure S3. a) Immunoblot analysis (upper panels) and p-FAK(tyr397) and p-Paxillin(tyr118) protein quantification (lower panels) performed on untreated or TGF-β treated PB and PB-PI3KC2α MDA-MB-468. b) Nocodazole washout assay was used to assess focal adhesion disassembly time (see Experimental Section). PB and PB-PI3KC2α MDA-MB-468 were fixed at indicated time points and immunostained for Vinculin. Representative pictures (left) and quantification of focal adhesions number per cell are shown (right). At least 6 images per time point were analyzed (5–10 cells per picture). Scale bar, 10 μm. All results are shown as mean of at least three independent experiments ± SEM (n.s., no significance, *P<0.05; **P<0.01).

Figure S4

a

b


c
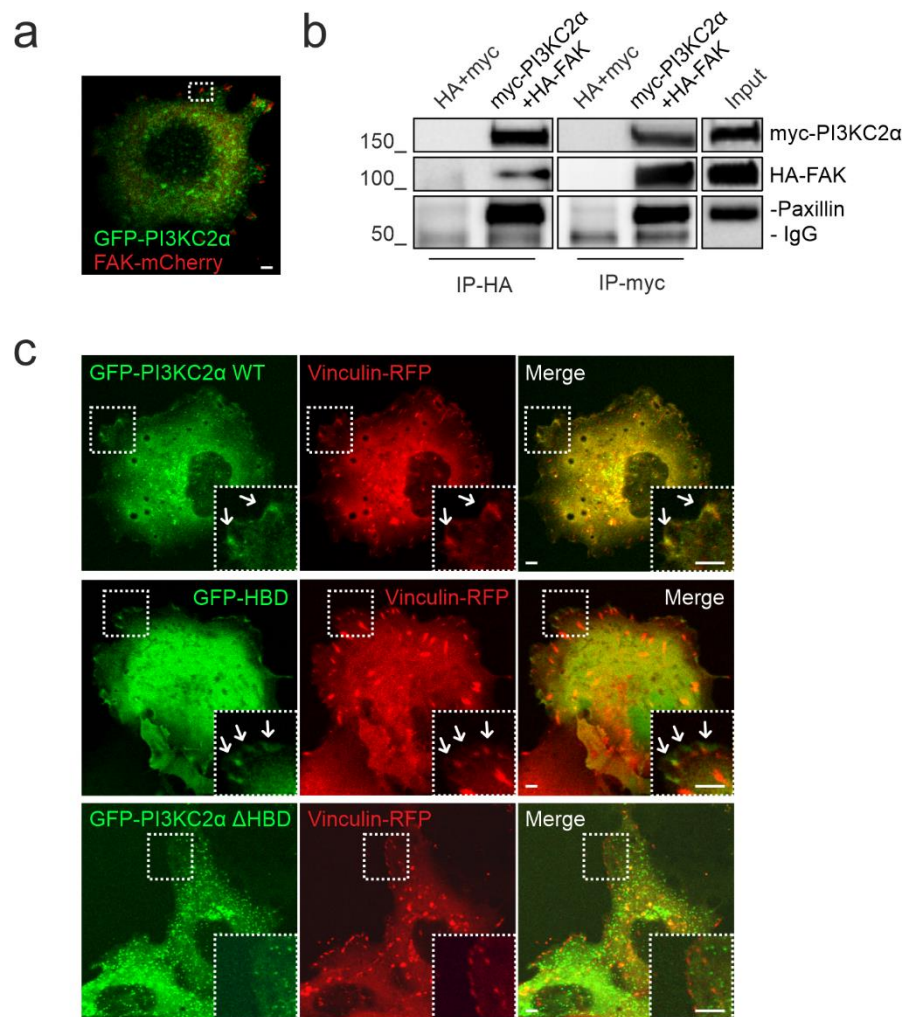
Figure S4. a) Representative picture of live cell imaging performed on MCF7 expressing FAK-mCherry (red) and GFP-PI3KC2α (green). b) Co-immunoprecipitation (Co-IP) experiment performed on HEK293T transfected with HA-FAK and myc-PI3KC2α. Bound proteins were blotted with anti-myc, anti HA and anti-paxillin antibodies. c) Live-cell imaging performed in COS7 expressing Vinculin-RFP (red) and GFP-PI3KC2a (WT, HBD or HBD deleted mutants).
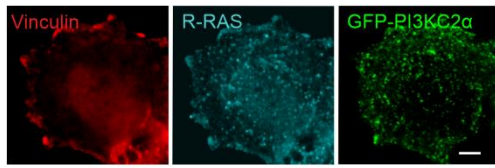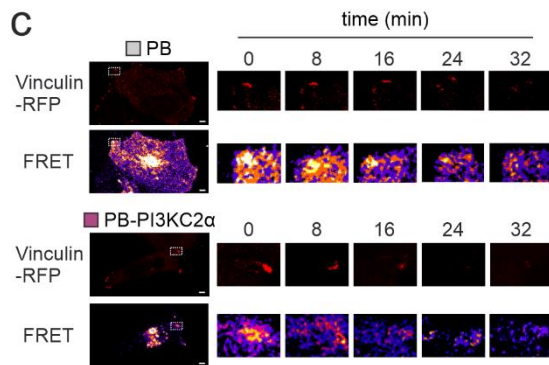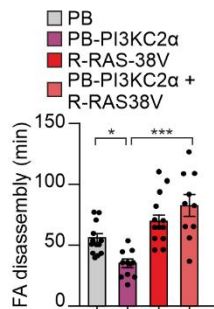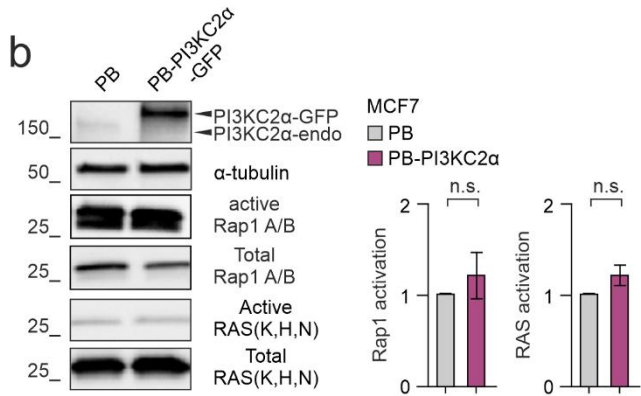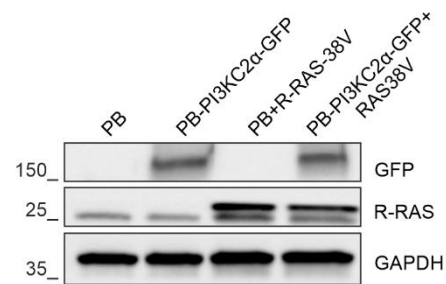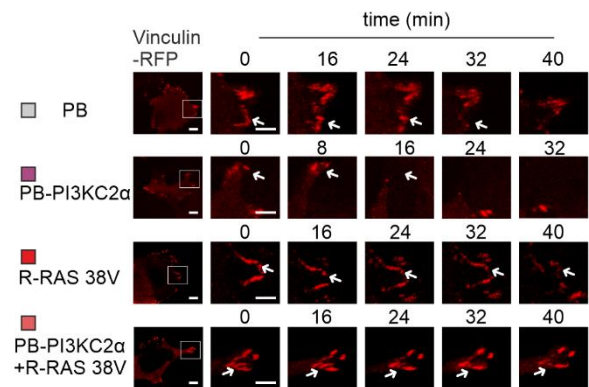
Figure S5. a) Immunofluorescence staining performed on MCF7 showing colocalization of GFP-PI3KC2α (green) with endogenous R-RAS (cyan) and Vinculin (red). b) Pull-down assay (left) and quantification (right) showing active Rap1A/B and RAS (K, H, N) in PB or PB-PI3KC2α MCF7. c) Representative pictures of R-RAS FRET ratio (pseudo-colour) on focal adhesion (red) during its disassembly performed in PB or PB-PI3KC2α MCF7 expressing Vinculin-RFP and Raichu-R-RAS FRET probe. d) Representative immunoblot showing overexpression of R-RAS-38v in PB or PB-PI3KC2α MCF7. e, f) Quantification (f) of focal adhesion disassembly time from time lapse (e) performed on living MCF7 cells expressing Vinculin-RFP and PB, PB-PI3KC2α, R-RAS 38V or PB-PI3KC2α + R-RAS 38V, respectively. n ≥ 10 focal adhesions from three independent experiments. All results are

shown as mean of at least three independent experiments ± SEM (n.s., no significance,

*P<0.05; ***P<0.001).

Figure S6
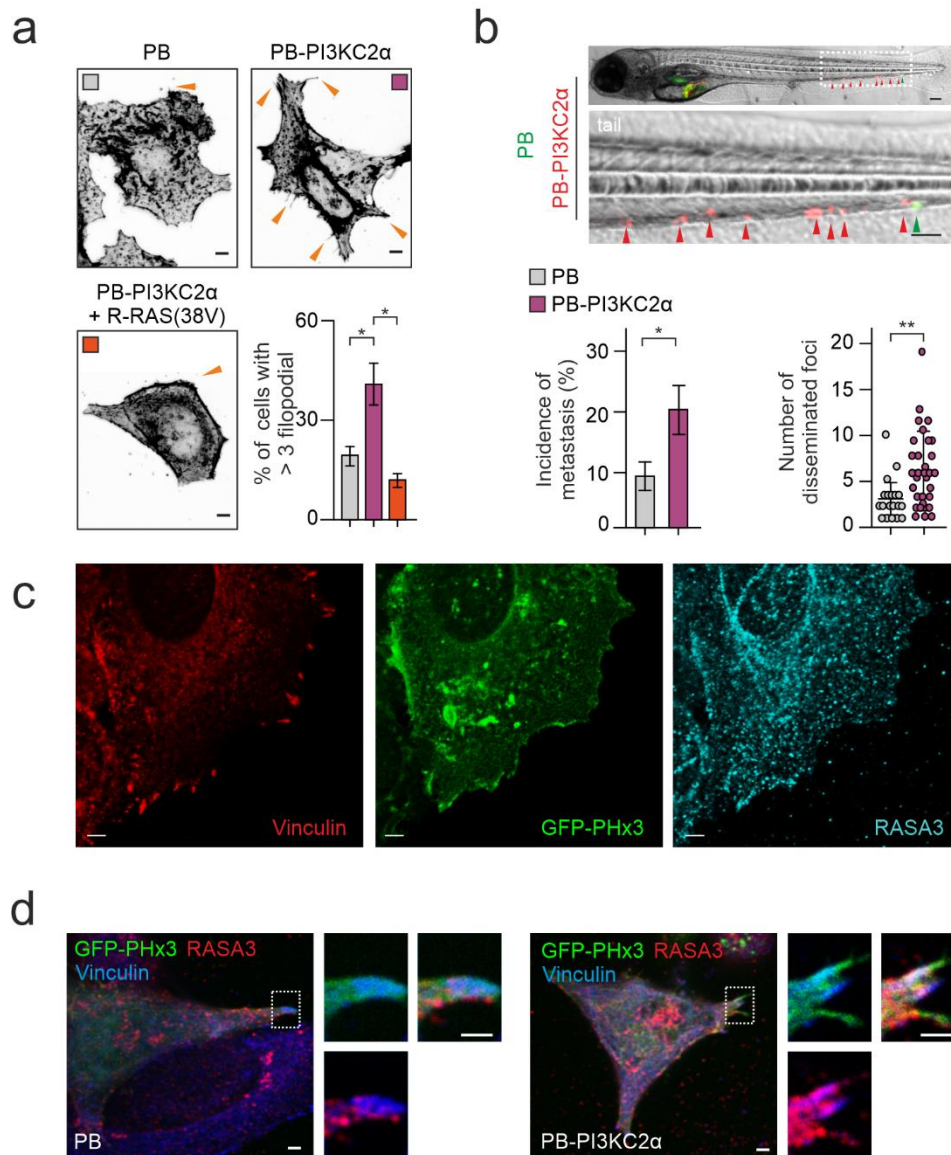
Figure S6. a) Percentage of cells showing filopodia number > 3 were counted in PB, PB-PI3KC2α and PB-PI3KC2α+R-RAS38V MCF7. n≥20 cells from at least three independent experiments. b) Representative pictures (upper panels) and quantification (bottom panels) showing number of disseminated foci and incidence of metastases in 48-hpf zebrafish injected with PB (Green) or PB-PI3KC2α (red) MCF7. Arrows indicate metastatic foci in zebrafish tail. n = 19 (PB), n = 32 (PB-PI3KC2α) zebrafish. Scale bar = 200 μm or 25 μm in enlarged sections. c) Immunofluorescence staining performed on MCF7 showing colocalization of GFP-TAPP1-PHx3 (green) with endogenous RASA3 (cyan) and FAK (red). Scale bar = 10

μm. d) Representative picture of RASA3 (red) at focal adhesion (vinculin, blue) performed on PB or PB-PI3KC2α MCF7 expressing GFP-TAPP1-PHx3 (green). n = 44 and n = 63 FAs for PB or PB-PI3KC2α respectively. Scale bar, 10 μm.

All results are shown as mean of at least three independent experiments ± SEM (n.s., no significance, *P<0.05; **P<0.01).

Table S1. Primers and probes used in quantitative RT-PCR.

Gene	Left primer(5'-3')	Right primer(5'-3')	Probe
CDH1	cccgggacaacgtttattac	gctggctcaagtcaaagtcc	#35
MMP1	gctaacctttgatgctataactacga	tttgtgcgcatgtagaatctg	#7
MMP9	gaaccaatctcaccgacagg	gccacccgagtgtaaccata	#6
Snai1	tacagcgagctgcaggact	atctccggaggtgggatg	#11
Snai2	tggttgcttcaaggacacat	gcaaatgctctgttgcagtg	#7
ZEB1	tgactatcaaaaggaagtcaatgg	gtgcaggagggacctcttta	#31

6. References

[1] F. Bray, J. Ferlay, I. Soerjomataram, R.L. Siegel, L.A. Torre, A. Jemal, Global cancer statistics 2018: GLOBOCAN estimates of incidence and mortality worldwide for 36 cancers in 185 countries, CA Cancer J Clin, 68 (2018) 394-424.

[2] R. Yeeravalli, A. Das, Molecular mediators of breast cancer metastasis, Hematol Oncol Stem Cell Ther, (2021).

[3] J.A. Broussard, D.J. Webb, I. Kaverina, Asymmetric focal adhesion disassembly in motile cells, Current opinion in cell biology, 20 (2008) 85-90.

[4] C. Collins, W.J. Nelson, Running with neighbors: coordinating cell migration and cell-cell adhesion, Current opinion in cell biology, 36 (2015) 62-70.

[5] A.J. Ridley, Life at the leading edge, Cell, 145 (2011) 1012-1022.

[6] D.J. Webb, J.T. Parsons, A.F. Horwitz, Adhesion assembly, disassembly and turnover in migrating cells -- over and over and over again, Nature cell biology, 4 (2002) E97-100.

[7] B.Y. Lee, P. Timpson, L.G. Horvath, R.J. Daly, FAK signaling in human cancer as a target for therapeutics, Pharmacol Ther, 146 (2015) 132-149.

[8] A.R. Hess, L.M. Postovit, N.V. Margaryan, E.A. Seftor, G.B. Schneider, R.E. Seftor, B.J. Nickoloff, M.J. Hendrix, Focal adhesion kinase promotes the aggressive melanoma phenotype, Cancer Res, 65 (2005) 9851-9860.

[9] T.M. Weiner, E.T. Liu, R.J. Craven, W.G. Cance, Expression of focal adhesion kinase gene and invasive cancer, Lancet, 342 (1993) 1024-1025.

[10] E. Hirsch, F. Gulluni, M. Martini, Phosphoinositides in cell proliferation and metabolism, Advances in biological regulation, 75 (2020) 100693.

[11] G. Di Paolo, P. De Camilli, Phosphoinositides in cell regulation and membrane dynamics, Nature, 443 (2006) 651-657.

[12] J. Hasegawa, E. Tokuda, T. Tenno, K. Tsujita, H. Sawai, H. Hiroaki, T. Takenawa, T. Itoh, SH3YL1 regulates dorsal ruffle formation by a novel phosphoinositide-binding domain, The Journal of cell biology, 193 (2011) 901-916.

[13] N. Prasad, R.S. Topping, S.J. Decker, Src family tyrosine kinases regulate adhesion-dependent tyrosine phosphorylation of 5'-inositol phosphatase SHIP2 during cell attachment and spreading on collagen I, Journal of cell science, 115 (2002) 3807-3815.

[14] Z. Feng, C.H. Yu, PI(3,4)P2-mediated membrane tubulation promotes integrin trafficking and invasive cell migration, Proceedings of the National Academy of Sciences of the United States of America, 118 (2021).

[15] M. Krause, A. Gautreau, Steering cell migration: lamellipodium dynamics and the regulation of directional persistence, Nature reviews. Molecular cell biology, 15 (2014) 577-590.

[16] V.P. Sharma, R. Eddy, D. Entenberg, M. Kai, F.B. Gertler, J. Condeelis, Tks5 and SHIP2 regulate invadopodium maturation, but not initiation, in breast carcinoma cells, Current biology : CB, 23 (2013) 2079-2089.

[17] M. Fukumoto, T. Ijuin, T. Takenawa, PI(3,4)P2 plays critical roles in the regulation of focal adhesion dynamics of MDA-MB-231 breast cancer cells, Cancer Sci, 108 (2017) 941-951.

[18] F. Gulluni, M. Martini, M.C. De Santis, C.C. Campa, A. Ghigo, J.P. Margaria, E. Ciraolo, I. Franco, U. Ala, L. Annaratone, D. Disalvatore, G. Bertalot, G. Viale, A. Noatynska, M. Compagno, S. Sigismund, F. Montemurro, M. Thelen, F. Fan, P. Meraldi, C. Marchio, S. Pece, A. Sapino, R. Chiarle, P.P. Di Fiore, E. Hirsch, Mitotic Spindle Assembly and Genomic Stability in Breast Cancer Require PI3K-C2alpha Scaffolding Function, Cancer cell, 32 (2017) 444-459 e447.

[19] W.T. Lo, Y. Zhang, O. Vadas, Y. Roske, F. Gulluni, M.C. De Santis, A.V. Zagar, H. Stephanowitz, E. Hirsch, F. Liu, O. Daumke, M. Kudryashev, V. Haucke, Structural basis of phosphatidylinositol 3-kinase C2alpha function, Nat Struct Mol Biol, 29 (2022) 218-228.

[20] P. Molina-Ortiz, T. Orban, M. Martin, A. Habets, F. Dequiedt, S. Schurmans, Rasa3 controls turnover of endothelial cell adhesion and vascular lumen integrity by a Rap1-dependent mechanism, PLoS genetics, 14 (2018) e1007195.

[21] S.J. Stehbens, M. Paszek, H. Pemble, A. Ettinger, S. Gierke, T. Wittmann, CLASPs link focal-adhesion-associated microtubule capture to localized exocytosis and adhesion site turnover, Nature cell biology, 16 (2014) 561-573.

[22] A.R. Jahejo, D. Zhang, S. Niu, R.A. Mangi, A. Khan, M.F. Qadir, A. Khan, H.C. Chen, W.X. Tian, Transcriptome-based screening of intracellular pathways and angiogenesis related genes at different stages of thiram induced tibial lesions in broiler chickens, BMC genomics, 21 (2020) 50.

[23] C.C. Campa, J.P. Margaria, A. Derle, M. Del Giudice, M.C. De Santis, L. Gozzelino, F. Copperi, C. Bosia, E. Hirsch, Rab11 activity and PtdIns(3)P turnover removes recycling cargo from endosomes, Nature chemical biology, (2018).

[24] A. Takaya, T. Kamio, M. Masuda, N. Mochizuki, H. Sawa, M. Sato, K. Nagashima, A. Mizutani, A. Matsuno, E. Kiyokawa, M. Matsuda, R-Ras regulates exocytosis by Rgl2/Rlf-mediated activation of RalA on endosomes, Molecular biology of the cell, 18 (2007) 1850-1860.

[25] K. Gumireddy, F. Sun, A.J. Klein-Szanto, J.M. Gibbins, P.A. Gimotty, A.J. Saunders, P.G. Schultz, Q. Huang, In vivo selection for metastasis promoting genes in the mouse, Proceedings of the National Academy of Sciences of the United States of America, 104 (2007) 6696-6701.

[26] I. Franco, F. Gulluni, C.C. Campa, C. Costa, J.P. Margaria, E. Ciraolo, M. Martini, D. Monteyne, E. De Luca, G. Germena, Y. Posor, T. Maffucci, S. Marengo, V. Haucke, M. Falasca, D. Perez-Morga, A. Boletta, G.R. Merlo, E. Hirsch, PI3K class II alpha controls spatially restricted endosomal PtdIns3P and Rab11 activation to promote primary cilium function, Developmental cell, 28 (2014) 647-658.

[27] I. Franco, J.P. Margaria, M.C. De Santis, A. Ranghino, D. Monteyne, M. Chiaravalli, M. Pema, C.C. Campa, E. Ratto, F. Gulluni, D. Perez-Morga, S. Somlo, G.R. Merlo, A. Boletta, E. Hirsch, Phosphoinositide 3-Kinase-C2alpha Regulates Polycystin-2 Ciliary Entry and Protects against Kidney Cyst Formation, Journal of the American Society of Nephrology : JASN, 27 (2016) 1135-1144.

[28] R.M. Neve, K. Chin, J. Fridlyand, J. Yeh, F.L. Baehner, T. Fevr, L. Clark, N. Bayani, J.P. Coppe, F. Tong, T. Speed, P.T. Spellman, S. DeVries, A. Lapuk, N.J. Wang, W.L. Kuo, J.L. Stilwell, D. Pinkel, D.G. Albertson, F.M. Waldman, F. McCormick, R.B. Dickson, M.D. Johnson, M. Lippman, S. Ethier, A. Gazdar, J.W. Gray, A collection of breast cancer cell lines for the study of functionally distinct cancer subtypes, Cancer cell, 10 (2006) 515-527.

[29] J. Barretina, G. Caponigro, N. Stransky, K. Venkatesan, A.A. Margolin, S. Kim, C.J. Wilson, J. Lehar, G.V. Kryukov, D. Sonkin, A. Reddy, M. Liu, L. Murray, M.F. Berger, J.E. Monahan, P. Morais, J. Meltzer, A. Korejwa, J. Jane-Valbuena, F.A. Mapa, J. Thibault, E. Bric-Furlong, P. Raman, A. Shipway, I.H. Engels, J. Cheng, G.K. Yu, J. Yu, P. Aspesi, Jr., M. de Silva, K. Jagtap, M.D. Jones, L. Wang, C. Hatton, E. Palescandolo, S. Gupta, S. Mahan, C. Sougnez, R.C. Onofrio, T. Liefeld, L. MacConaill, W. Winckler, M. Reich, N. Li, J.P. Mesirov, S.B. Gabriel, G. Getz, K. Ardlie, V. Chan, V.E. Myer, B.L. Weber, J. Porter, M. Warmuth, P. Finan, J.L. Harris, M. Meyerson, T.R. Golub, M.P. Morrissey, W.R. Sellers, R. Schlegel, L.A. Garraway, The Cancer Cell Line Encyclopedia enables predictive modelling of anticancer drug sensitivity, Nature, 483 (2012) 603-607.

[30] C.J. Aslakson, F.R. Miller, Selective events in the metastatic process defined by analysis of the sequential dissemination of subpopulations of a mouse mammary tumor, Cancer Res, 52 (1992) 1399-1405.

[31] C. Khanna, K. Hunter, Modeling metastasis in vivo, Carcinogenesis, 26 (2005) 513-523.

[32] S. Seetharaman, S. Etienne-Manneville, Cytoskeletal Crosstalk in Cell Migration, Trends in cell biology, 30 (2020) 720-735.

[33] S. Aki, K. Yoshioka, Y. Okamoto, N. Takuwa, Y. Takuwa, Phosphatidylinositol 3-kinase class II alpha-isoform PI3K-C2alpha is required for transforming growth factor beta-induced Smad signaling in endothelial cells, The Journal of biological chemistry, 290 (2015) 6086-6105.

[34] M.L. Gardel, I.C. Schneider, Y. Aratyn-Schaus, C.M. Waterman, Mechanical integration of actin and adhesion dynamics in cell migration, Annu Rev Cell Dev Biol, 26 (2010) 315-333.

[35] X.Q. Fang, X.F. Liu, L. Yao, C.Q. Chen, J.F. Lin, Z.D. Gu, P.H. Ni, X.M. Zheng, Q.S. Fan, Focal adhesion kinase regulates the phosphorylation protein tyrosine phosphatase-alpha at Tyr789 in breast cancer cells, Mol Med Rep, 11 (2015) 4303-4308.

[36] T.B. Deramaudt, D. Dujardin, A. Hamadi, F. Noulet, K. Kolli, J. De Mey, K. Takeda, P. Ronde, FAK phosphorylation at Tyr-925 regulates cross-talk between focal adhesion turnover and cell protrusion, Molecular biology of the cell, 22 (2011) 964-975.

[37] J. Chen, K.A. Gallo, MLK3 regulates paxillin phosphorylation in chemokine-mediated breast cancer cell migration and invasion to drive metastasis, Cancer Res, 72 (2012) 4130-4140.

[38] A. Hamadi, M. Bouali, M. Dontenwill, H. Stoeckel, K. Takeda, P. Ronde, Regulation of focal adhesion dynamics and disassembly by phosphorylation of FAK at tyrosine 397, Journal of cell science, 118 (2005) 4415-4425.

[39] E.J. Ezratty, M.A. Partridge, G.G. Gundersen, Microtubule-induced focal adhesion disassembly is mediated by dynamin and focal adhesion kinase, Nature cell biology, 7 (2005) 581-590.

[40] H. Wang, W.T. Lo, A. Vujicic Zagar, F. Gulluni, M. Lehmann, L. Scapozza, V. Haucke, O. Vadas, Autoregulation of Class II Alpha PI3K Activity by Its Lipid-Binding PX-C2 Domain Module, Molecular cell, 71 (2018) 343-351 e344.

[41] B.D. Goulden, J. Pacheco, A. Dull, J.P. Zewe, A. Deiters, G.R.V. Hammond, A high-avidity biosensor reveals plasma membrane PI(3,4)P2 is predominantly a class I PI3K signaling product, The Journal of cell biology, 218 (2019) 1066-1079.

[42] X. Li, M. Edwards, K.F. Swaney, N. Singh, S. Bhattacharya, J. Borleis, Y. Long, P.A. Iglesias, J. Chen, P.N. Devreotes, Mutually inhibitory Ras-PI(3,4)P2 feedback loops mediate cell migration, Proceedings of the National Academy of Sciences of the United States of America, 115 (2018) E9125-E9134.

[43] J. Furuhjelm, J. Peranen, The C-terminal end of R-Ras contains a focal adhesion targeting signal, Journal of cell science, 116 (2003) 3729-3738.

[44] H.W. Jeong, J.O. Nam, I.S. Kim, The COOH-terminal end of R-Ras alters the motility and morphology of breast epithelial cells through Rho/Rho-kinase, Cancer Res, 65 (2005) 507-515.

[45] L. Kwong, M.A. Wozniak, A.S. Collins, S.D. Wilson, P.J. Keely, R-Ras promotes focal adhesion formation through focal adhesion kinase and p130(Cas) by a novel mechanism that differs from integrins, Molecular and cellular biology, 23 (2003) 933-949.

[46] G. Singh, D. Hashimoto, X. Yan, J. Helft, P.J. Park, G. Ma, R.F. Qiao, C.R. Kennedy, S.H. Chen, M. Merad, A.M. Chan, R-Ras is required for murine dendritic cell maturation and CD4+ T-cell priming, Blood, 119 (2012) 1693-1701.

[47] I. Fujita, A. Shitamukai, F. Kusumoto, S. Mase, T. Suetsugu, A. Omori, K. Kato, T. Abe, G. Shioi, D. Konno, F. Matsuzaki, Endfoot regeneration restricts radial glial state and

prevents translocation into the outer subventricular zone in early mammalian brain development, Nature cell biology, 22 (2020) 26-37.

[48] R. Fior, V. Povoa, R.V. Mendes, T. Carvalho, A. Gomes, N. Figueiredo, M.G. Ferreira, Single-cell functional and chemosensitive profiling of combinatorial colorectal therapy in zebrafish xenografts, Proceedings of the National Academy of Sciences of the United States of America, 114 (2017) E8234-E8243.

[49] A. Hennig, R. Markwart, M.A. Esparza-Franco, G. Ladds, I. Rubio, Ras activation revisited: role of GEF and GAP systems, Biol Chem, 396 (2015) 831-848.

[50] T.N. Durrant, S.F. Moore, A.L. Bayliss, Y. Jiang, E.W. Aitken, M.C. Wilson, K.J. Heesom, I. Hers, Identification of PtdIns(3,4)P2 effectors in human platelets using quantitative proteomics, Biochim Biophys Acta Mol Cell Biol Lipids, 1865 (2020) 158575.

[51] F. Gulluni, M.C. De Santis, J.P. Margaria, M. Martini, E. Hirsch, Class II PI3K Functions in Cell Biology and Disease, Trends in cell biology, (2019).

[52] D. Tiosano, H.N. Baris, A. Chen, M.M. Hitzert, M. Schueler, F. Gulluni, A. Wiesener, A. Bergua, A. Mory, B. Copeland, J.G. Gleeson, P. Rump, H. van Meer, D.A. Sival, V. Haucke, J. Kriwinsky, K.X. Knaup, A. Reis, N.N. Hauer, E. Hirsch, R. Roepman, R. Pfundt, C.T. Thiel, M.S. Wiesener, M.G. Aslanyan, D.A. Buchner, Mutations in PIK3C2A cause syndromic short stature, skeletal abnormalities, and cataracts associated with ciliary dysfunction, PLoS genetics, 15 (2019) e1008088.

[53] K. Yoshioka, K. Yoshida, H. Cui, T. Wakayama, N. Takuwa, Y. Okamoto, W. Du, X. Qi, K. Asanuma, K. Sugihara, S. Aki, H. Miyazawa, K. Biswas, C. Nagakura, M. Ueno, S. Iseki, R.J. Schwartz, H. Okamoto, T. Sasaki, O. Matsui, M. Asano, R.H. Adams, N. Takakura, Y. Takuwa, Endothelial PI3K-C2alpha, a class II PI3K, has an essential role in angiogenesis and vascular barrier function, Nature medicine, 18 (2012) 1560-1569.

[54] L. Di Leo, V. Bodemeyer, F.M. Bosisio, G. Claps, M. Carretta, S. Rizza, F. Faienza, A. Frias, S. Khan, M. Bordi, M.P. Pacheco, J. Di Martino, J.J. Bravo-Cordero, C.J. Daniel, R.C. Sears, M. Donia, D.H. Madsen, P. Guldberg, G. Filomeni, T. Sauter, C. Robert, D. De Zio, F. Cecconi, Loss of Ambra1 promotes melanoma growth and invasion, Nature communications, 12 (2021) 2550.

[55] N. Nonpanya, K. Sanookpan, N. Sriratanasak, C. Vinayanuwattikun, D. Wichadakul, B. Sritularak, P. Chanvorachote, Artocarpin Targets Focal Adhesion Kinase-Dependent Epithelial to Mesenchymal Transition and Suppresses Migratory-Associated Integrins in Lung Cancer Cells, Pharmaceutics, 13 (2021).

[56] V.M. Golubovskaya, Targeting FAK in human cancer: from finding to first clinical trials, Frontiers in bioscience (Landmark edition), 19 (2014) 687-706.

[57] L. Gozzelino, M.C. De Santis, F. Gulluni, E. Hirsch, M. Martini, PI(3,4)P2 Signaling in Cancer and Metabolism, Frontiers in oncology, 10 (2020) 360.

[58] T. Ijuin, Phosphoinositide phosphatases in cancer cell dynamics-Beyond PI3K and PTEN, Semin Cancer Biol, 59 (2019) 50-65.

[59] S. Schurmans, S. Polizzi, A. Scoumanne, S. Sayyed, P. Molina-Ortiz, The Ras/Rap GTPase activating protein RASA3: from gene structure to in vivo functions, Advances in biological regulation, 57 (2015) 153-161.

[60] S. Yarwood, D. Bouyoucef-Cherchalli, P.J. Cullen, S. Kupzig, The GAP1 family of GTPase-activating proteins: spatial and temporal regulators of small GTPase signalling, Biochemical Society transactions, 34 (2006) 846-850.

[61] B. Sot, C. Kotting, D. Deaconescu, Y. Suveyzdis, K. Gerwert, A. Wittinghofer, Unravelling the mechanism of dual-specificity GAPs, The EMBO journal, 29 (2010) 1205-1214.

[62] Y. Zhang, R. Sugiura, Y. Lu, M. Asami, T. Maeda, T. Itoh, T. Takenawa, H. Shuntoh, T. Kuno, Phosphatidylinositol 4-phosphate 5-kinase Its3 and calcineurin Ppb1 coordinately

regulate cytokinesis in fission yeast, The Journal of biological chemistry, 275 (2000) 35600-35606.

[63] M.A. Wozniak, L. Kwong, D. Chodniewicz, R.L. Klemke, P.J. Keely, R-Ras controls membrane protrusion and cell migration through the spatial regulation of Rac and Rho, Molecular biology of the cell, 16 (2005) 84-96.

7. Acknowledgement

Torino   Day   Night

Moncenisio   Ceresole Reale

Dolomiti   Genova

Cinque Terre

Capri

Cibo e vino